CONTROL OF BOUNCING IN RF MEMS SWITCHES USING DOUBLE ELECTRODE

Thesis by

Farhan Abdul Rahim

In Partial Fulfillment of the Requirements

For the Degree of

Master of Science

King Abdullah University of Science and Technology

Thuwal, Kingdom of Saudi Arabia

May 2014

EXAMINATION COMMITTEE APPROVALS FORM

The thesis of Farhan Abdul Rahim is approved by the examination committee.

Committee Chairperson Mohammed I. Younis

Committee Member Sigurdur Thoroddsen

Committee Member Christian G. Claudel

CONTROL OF BOUNCING IN RF MEMS SWITCHES USING DOUBLE ELECTRODE

Farhan Abdul Rahim

ABSTRACT

MEMS based mechanical switches are seen to be the likely replacements for CMOS based switches due to the several advantages that these mechanical switches have over CMOS switches. Mechanical switches can be used in systems under extreme conditions and also provide more reliability and cause less power loss. A major problem with mechanical switches is bouncing. Bouncing is an undesirable characteristic which increases the switching time and causes damage to the switch structure affecting the overall switch life. This thesis proposes a new switch design that may be used to mitigate bouncing by using two voltage sources using a double electrode configuration. The effect of many switch's tunable parameters is also discussed and an effective tuning technique is also provided. The results are compared to the current control schemes in literature and show that the double electrode scheme is a viable control option.

ACKNOWLEDGEMENTS

I would like to thank my committee chair, Dr. Mohammed I. Younis and my committee members, Sigurdur Thoroddsen, and Christian G. Claudel, for their guidance and support throughout the course of this research.

My appreciation also goes to my friends and colleagues who helped me out in any way possible during my research and who always helped me achieve my full potential.

Last but not the least I would like to thank my parents for their support and prayers which helped me keep going forward.

TABLE OF CONTENTS

Page

LIST OF ILLUSTRATIONS

LIST OF TABLES

Chapter 1.
Introduction

MEMS are present in almost all of everyday objects. They are present in mobile phones, toys, appliances and even car tires. The low cost of batch processed devices coupled with high reliability and extremely small scale makes MEMS devices a viable option for mass scale consumer goods industry. Many MEMS devices are present as sensors that have capability of measuring several physical quantities. Velocity, temperature humidity and luminosity are some of the few quantities that can be monitored using MEMS.

One of the major areas of work in MEMS includes ohmic switches. The switch basic design is based on the model of already prevalent CMOS based solid state switches known as MOSFETS. A typical switch is composed of a gate, drain and a source. MEMS switches are similar in this regard having same three components. However, the method of transferring the signal and actuation is done through mechanical means by the use of a cantilever based design. These types of switches have several advantages over their CMOS based counterparts. Power efficiency is one main advantage as these MEMS based switches can operate at lower power inputs .Furthermore , as solid state switches are made smaller and smaller in line with the decreasing size of consumer electronics, the phenomenon of tunneling currents has caused large leakage currents causing loss of energy and the device never being in the off state completely. Compared to that , researchers have shown that leakage

currents are up to 10^-15 times less in case of MEMS switches making them an ideal next step for next generation small scale consumer devices [1].

However, current level in MEMS switching technology makes it hard for the switches to be used in high frequency applications. This is due to the physical limitation on the connection time between the cantilever tip and the gate. This is made worse by the presence of the phenomenon known as bouncing. Bouncing is defined as the discontinuities in the switching process after the switch has made first contact with the substrate. Bouncing can be hazardous for the switch.

Bouncing is not very well understood and several authors have modeled bouncing with different methodologies. However it is shown that bouncing does not follow the well understood model of mechanical bounce and is highly nonlinear and dependent on the condition of the substrate and the damping apart from the other parameters present. There are several problems associated with bouncing that make it an undesirable phenomenon. Bouncing increases the switching time which is problematic for high frequency applications such as in RF MEMS. Furthermore, the high impact velocity damages the switch itself and the substrate by causing local hardening and pitting of the substrate material. Furthermore the heat produced in the impact might cause the metal in the switch to weld reducing the effective life of the switch. Several authors have discussed methods to reduce bouncing which range from open loop control, changing the structure of the tip and the substrate to using different materials altogether [1-6].

By reducing bouncing, it is possible to increase the lifetime of the switch by several years. It also means improving the switch dynamics by allowing faster and more responsive switches. Reliability of these switches will also be improved since bouncing tends to destroy switches quite randomly in large ensemble of switches.

One way to control bouncing is to apply a secondary pulse that can slow down the beam and reduce bouncing. Application of such a pulse is hard and may require complex circuitry if only a signal pulse is input to the system. In this thesis, we propose an alternative solution, which is to use two electrode with one electrode used as the actuation electrode and the other used as a control electrode as shown in figure (1). The actuation and control voltages can be used to reliably change the dynamics of the system and allow users to choose landing time and landing velocities easily , making tuning easy especially for a large ensemble of switches.

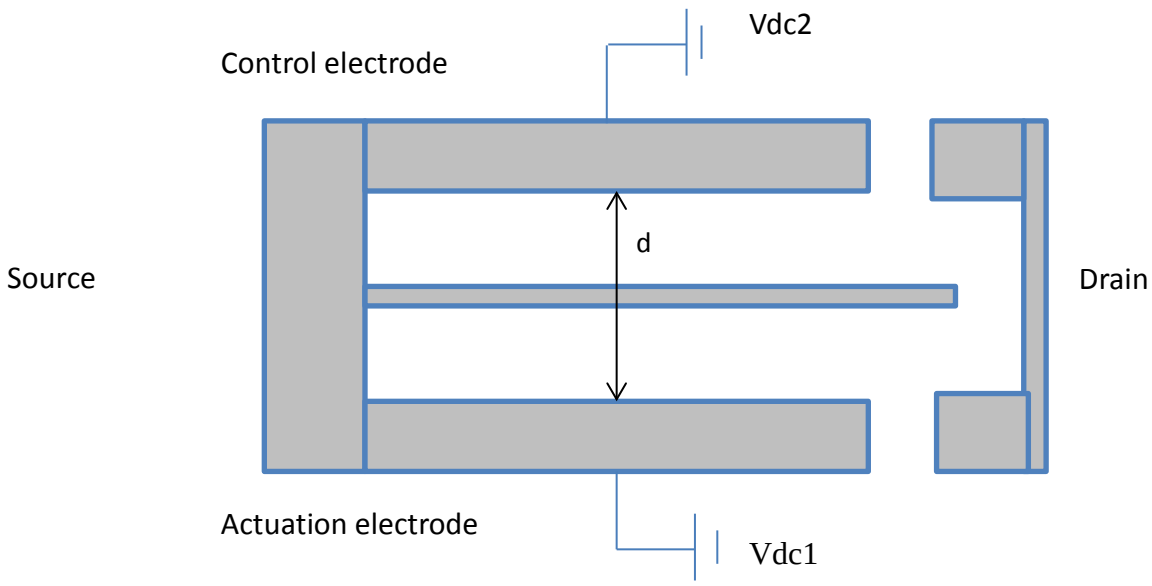

Figure 1: Proposed double electrode model

Chapter 2.
Literature Review

2.1 Models for Bouncing

Bouncing causes the closing time of the switch to be increased meaning that switches currently can only function for low frequency applications. Bouncing also causes damage to the substrate and to the cantilever by way of pitting, hardening of the surface and sometimes even welding due to heat created in the impact [1].

Many techniques have been proposed by authors to simulate the effect of bouncing. In all techniques, the authors seek to capture the dynamics of the system using the key variables. Various techniques have been used to model the effect of bouncing. McCarthy *et al* [2] and Do *et al* [3] used Euler Bernoulli beam mode to simulate the beam dynamics. Bouncing was simulated by inserting a spring at the point of contact and equating the spring to the shear force at the beam. However, only McCarthy *et al* [2] did a discussion on the non-linearity of the contact and the spring. Figure (2) shows the result of the model for different voltages. The damping was assumed to be dominated by squeeze film damping and modeled using the Reynolds equation. The calculation was done using finite time difference methods.

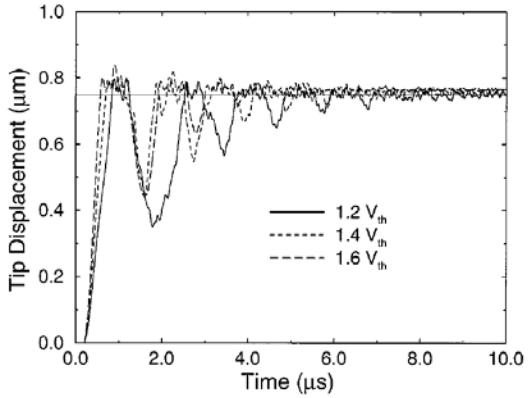

Figure 2: Bouncing simulation using a beam model [2]

Other authors used lumped mass parameter models favoring springs to simulate bouncing. The basic model found in [4-6] was a spring mass model of the form in figure (3) which was used to model different designs of switches. The model was based on a 3D design and the lumped mass parameter model also in figure (4). Several other designs are modeled using the same technique by varying the stiffness and the damping of the system. The model is a single degree of freedom system which equates the difference of the nonlinear electrostatic force to the linear stiffness force to the dynamic equation of the system.

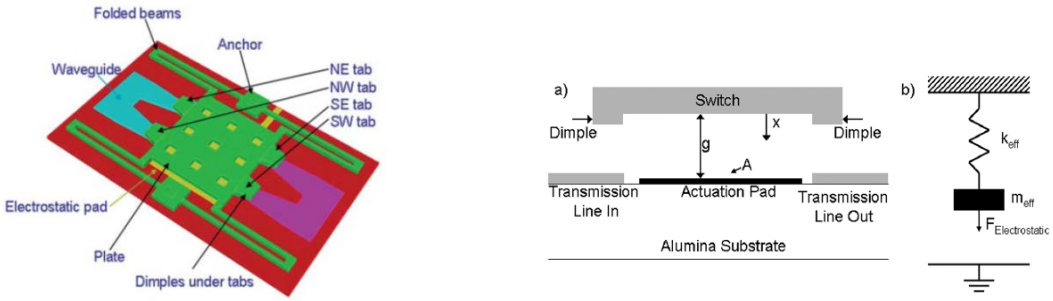

Figure 3: 3D image of th RF switch and the lumped mass model for free mode[4]

Figure 4: SEM image of RF switch and lumped mass model [5]

To correctly simulate bouncing, many authors such as [2, 3] used a second model when the spring comes in contact with the substrate. The effective stiffness, mass and the damping are recalibrated and acquired from either 3D model, optimization techniques and/or empirically obtained as in [5]. Figure (3) depicts the model as well as an SEM of the actual switch used with updated damping and stiffness.

The updated model was activated in different ways by different authors. Authors in [5] chose to only activate the model once and simulate the entire bouncing through the second model with forcing equated to 0, others [2], [3] reverted back to the free spring mass model when the mass left the substrate. Furthermore many authors considered the substrate ridged which is not going to be the case in this study.

Some authors presented more rigorous representation than a simple spring mass model. Peschot *et al* [7] presented a theory assuming the tip of the cantilever beam to be spherical and assuming bouncing to be mechanical bouncing with a constant coefficient of restitution between bounces. The group tested the theory by applying point loads using an AFM setup and Nano indenter setups as shown in figure (5).

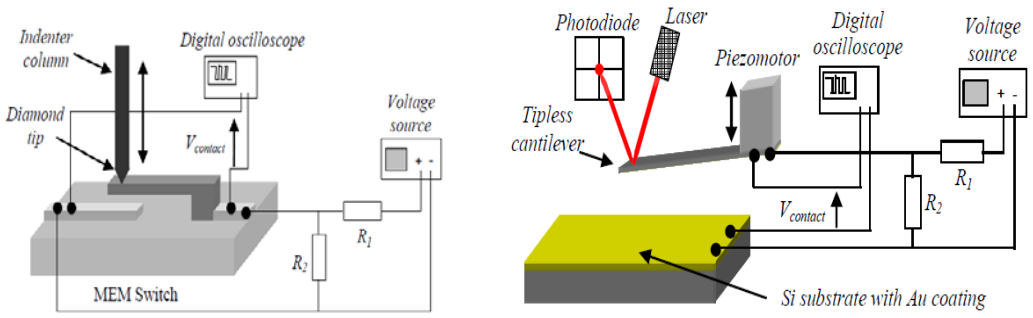

Figure 5: testing schematics for AFM and Nano indenter testing [7]

The measurements and further analysis [7] indicated that bouncing phenomenon is highly nonlinear and cannot be explained by simple mechanical bouncing theory. The research also used Casimir forces for very short distance to explain the phenomenon of electrical bounce which is only nanometers in height. Figure (6) shows the dominant forces and their ranges for a mechanical switch [7].

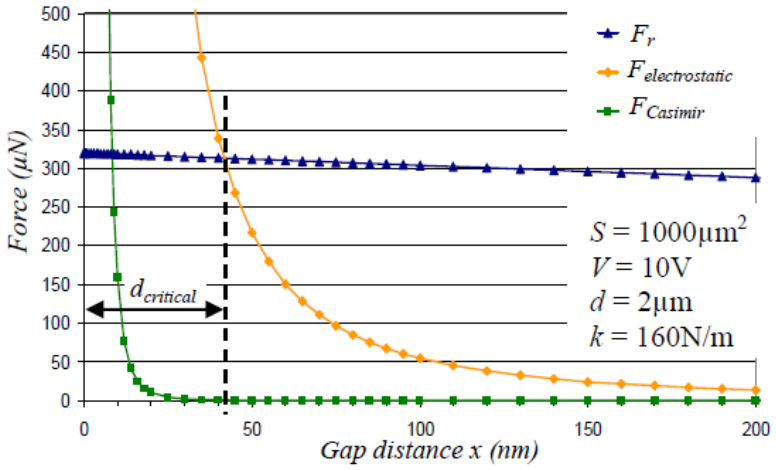

Figure 6: Forces affecting the beam with respect to the distance [7]

Recently, Tung *et al* [8] modeled the bouncing using reduced order modeling and squeeze film damping. The final simulation and testing showed that using 2 modes in the simulation captures the real dynamics of the system as the actually bouncing has several short spaced impacts during the actual impact. The transient excitation of the spring can be thus accurately captured by using a 2^{nd} mode in the reduced order model. The authors showed the dependence of contact stiffness and actuation voltage to final bouncing characteristics.

2.2 Control of Bouncing

Lots of research have been presented on methods aiming to reduce bouncing. Various forms of control including pulse shaping functions, change in mechanical switch circuitry and changing the shape tip and the substrate have been presented as methods to mitigate the effect of bouncing.

Jain *et al* [9] introduced two new novel ways to reduce the speed of the switch during bounce. The authors proposed introducing a resistor in series with the switch voltage source. The resulting analysis showed that the resistor did not affect the pull in characteristic of the switch during the initial phase, due to low transient current at the start. However during the stage when contacting the substrate, a large transient current across the resistor helped dissipate most of the kinetic energy reducing the speed of the switch by almost 50% in some cases. This system works on the principle of negative feedback control but the circuitry is simple and robust. This control, termed 'resistive braking', can be used well in a large ensemble of switches due to its simple design. Figure (7) shows another method proposed [9], to

pattern the substrate as electrically connected cylinders or other similar shapes that could be easily fabricated. The fringing fields of each structure are quite close during the initial stages of pull in; hence the pull in voltage remains roughly the same. However as the switch tip gets closer, the fringing fields rapidly diverge reducing the available potential energy that may be converted to kinetic energy, hence causing a reduction in speed of the tip. Figure (7) also shows the pattering as well as speed reduction as a function of separation (g), fractal dimension (DF) with reference of speed and distance travelled.

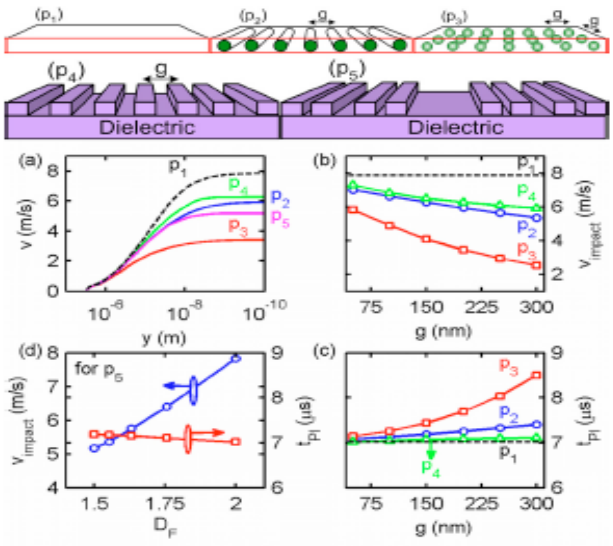

Figure 7: Different substrate shapes and effect of different parameters in landing times and landing velocity [9]

Another method to control bouncing is the input pulse shaping .The current literature presents variety of different ways in which the voltage wave can be manipulated to ensure that the switch closing time and the bouncing speed are minimized. Sumali *et al* [1] introduced a dual pulse waveform that allows the switch

to close while reducing the speed of the impact on the substrate, hence reducing bounce of the switch. The dual pulse wave and the corresponding system, as shown in figure (8), have a high voltage in the start which causes the switch to move towards the substrate at a high velocity. After the initial phase, the voltage is set to low to allow the switch to slow down due to the intrinsic damping as well as the squeeze film damping [1]. On reaching the substrate, a holding voltage is applied that ensure the mechanical restoring forces present in the switch not moving the switch back to the initial stage. Different forms of the same rectangular wave were tested in trapezoidal and rounded waveform to understand which form of the wave provided the least velocity at impact. Rounded waveforms were seen to perform the best due to the rectangular waveform being hard to generate exactly in the experiment.

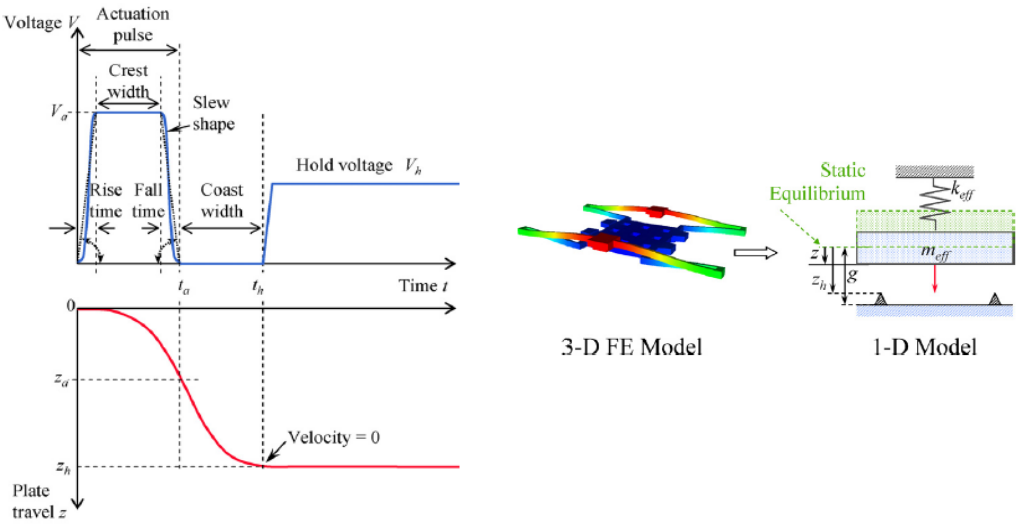

Figure 8: Parameters of input wave for open loop control and 3D model for the RF switch used in the paper [1]

Several authors have worked on methodologies of refining and selecting the best parameters for the dual pulse wave. Blecke et al [5] introduced a close loop control system to iteratively select parameters for the dual pulse wave. The system can be started off from a low voltage to ensure switch safety. The method has been shown experimentally to reduce switch closure time and velocity of impact by more than 50 % in each case. Figure (9) shows the dynamics of the switch for some iterative cycles.

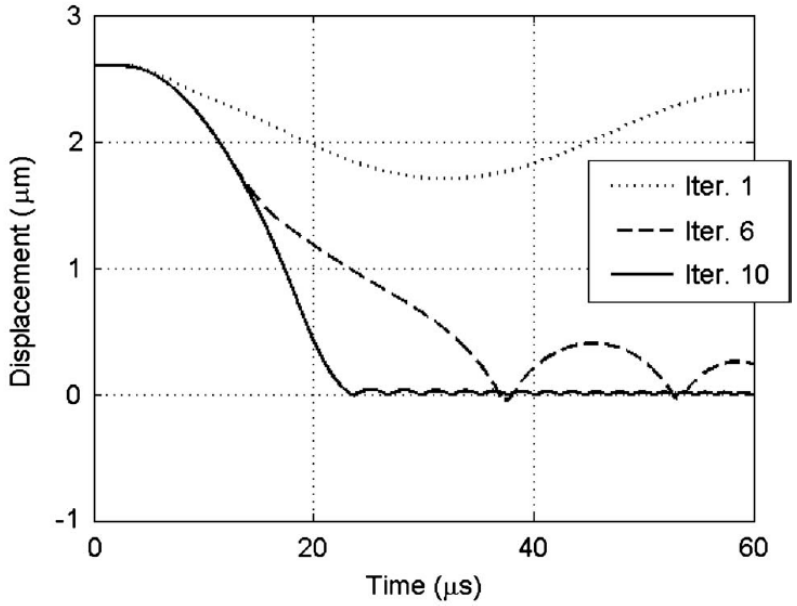

Figure 9: Beam dynamics for different iterations of self-learning control [5]

On the other hand, Do *et al* [3] developed an analytical method based on energy consideration for selecting the parameters of the dual pulse wave. The paper then introduces an adaptive control that changed the effective gap in the force equation

to obtain new parameters for the equation. Lai *et al* [6] compared the different waveforms used in changing the actuation voltage for MEMS switches and their effect on the life of these switches (by comparing dielectric charging and bouncing caused by each waveform). The four types of waveforms discussed in the paper were namely step voltage (ST), dual pulse actuation voltage (DP), exponentially increased dual pulse voltage (EDP) and soft landing voltage (SL). The author concluded that ST was the worst both in closing time, bouncing mitigation and dielectric charging. SL was the best for switching time bouncing mitigation but required complex tuning and feedback control to implement. On the other hand EDP was best amongst the tested waves in reducing dielectric charging, but had the slowest time amongst all tailored waveforms. EDP and DP were less sensitive to changes in pull in voltage variation then SL and hence were found to be much easier to implement for a switch.

Spasos *et al* [10] presented in their paper a description of two presented techniques known as the charge control (resistive damping) and voltage control based on an open loop statically method to control bouncing called the Taguchis optimization technique. The charge control presented is similar to those in [8] that it uses a constant current source and a resistor in series with the switch. The paper also presented a new hybrid technique which was mixture of the two existing techniques explained above. The voltage technique based on Taguchi's technique allowed for a tailored pulse that reduced impact velocity by 41.6%, impact force by 20% and the maximum bouncing displacement by 70% as compared to a similar tailored pulse

calculated using analytical technique. The paper also concluded that the charge control method was inappropriate for the rise time as only one regime (rise or fall time) may be tuned using the charge control. The hybrid technique was a mixture of the two which improved on all the important parameters with a minor increase in the closing time of the switch.

2.3 Switch Design

More recently, a double electrode model was designed by Dadgour *et al* [11] to present a universal NAND NOR gate. A similar switch design may be implemented in the MEMS scale to obtain a double electrode switch.

Chapter 3.
Theory and Operations

Bouncing and the operation of the device may be modeled by two separate theories. We can use the Euler Bernoulli beam theory to model the dynamics of the system or use the lumped mass parameter model. Both models have their advantages and disadvantages. While Euler Bernoulli theory provides the deflection of every point on the beam with respect to time, lumped mass parameter model can only be used for tip displacement (or any other chosen point) on one particular derived model. Also, lumped parameter model is computationally much faster and easier to implement. However, the beam model is more accurate compared to the lumped mass model. In this thesis, both systems are implemented for single and double beam models.

3.1 Beam Model for Single Electrode

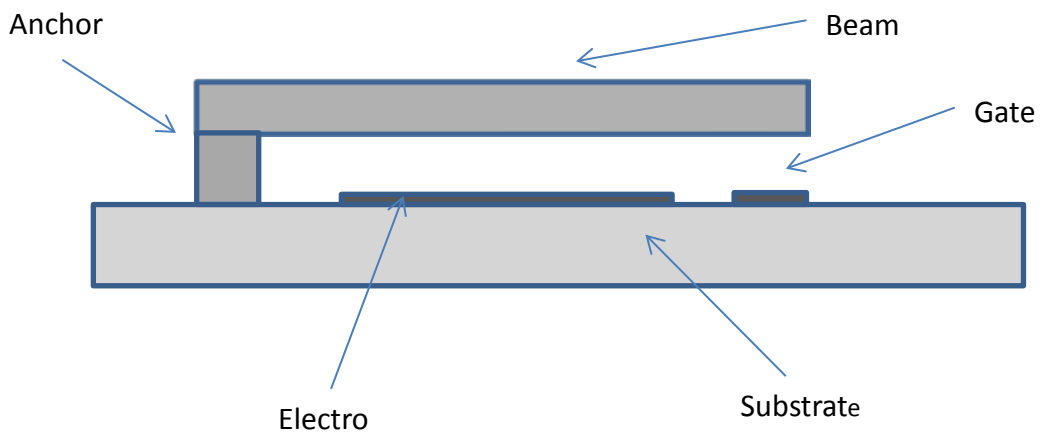

Figure 10: Single electrode beam cross sectional design

To derive the linear equation of motion of the beam, we start from a free body diagram of the beam cross section. The following equation is taken from [12]:

$$\frac{\partial^2}{\partial x^2}\left(EI\frac{\partial^2 w}{\partial x^2}\right) + \rho A\frac{\partial^2 w}{\partial t^2} + c\frac{\partial w}{\partial t} = F \tag{1}$$

Where E is the young's modulus, I is the moment of inertia, w is the beam deflection, ρ and A are the density and area respectively, c is the damping coefficient and F is the forcing term. Using the above equation (1), we can derive the dynamic characteristic of the bouncing and deflection of the beam using specific boundary condition. For a cantilever beam we apply the no displacement and no gradient boundary condition at $x=0$, and no moment and shear force at $x=L$.

3.1.1 Calculating the Eigenvalue and the Eigenmode

Next, we solve the above equation to simulate bouncing in the system. To solve for the dynamics, we assume the function as a separable variable of the form

$$w(x,t) = \sum \phi(x)u(t) \tag{2}$$

Where $w(x,t)$ is the deflection, $\phi(x)$ is the modeshape and $u(t)$ is the modal coordinate variable.

a. No Contact Regime

In this case, the $\phi(x)$ is of a free cantilever beam and hence can be assumed to be of the form [12],

$$\phi(x) = A\cos(\beta x) + B\sin(\beta x + + C\cosh(\beta x) + D\sinh(\beta x) \tag{3}$$

The following boundary conditions are implemented for a cantilever beam

$$\phi(0)=0 \qquad \phi'(0)=0 \qquad \phi''(l)=0 \qquad EI\phi'''(l)=0 \tag{4}$$

Will give a system of equations of the form

$$\begin{bmatrix} 1 & 0 & 1 & 0 \\ 0 & 1 & 0 & 1 \\ -\cos(\beta l) & -\sin(\beta x) & \cosh(\beta l) & \sinh(\beta l) \\ \sin(\beta l) & -\cos(\beta l) & \sinh(\beta l) & \cosh(\beta l) \end{bmatrix} \begin{bmatrix} A \\ B \\ C \\ D \end{bmatrix} = \begin{bmatrix} 0 \\ 0 \\ 0 \\ 0 \end{bmatrix} \tag{5}$$

To avoid a trivial solution, we assume the first matrix to be singular and set the determinant of the matrix equal to 0. The determinant gives the equation of this form:

$$\cos(\beta l)^2 + \cosh(\beta l)^2 + \sin(\beta l)^2 - \sinh(\beta l)^2 + 2 * \cos(\beta l) * \cosh(\beta l) = 0 \tag{6}$$

We solve for the values of βl which correspond to each mode shape of the beam.

Since the matrix is assumed to be singular, *Ax=b* either has no solution's or infinitely many solutions. We assume the latter case.

After nondimensionalization and solution of the coefficients A, B, C and D in terms of one of the variable we obtain the equation [6].

$$\phi_n(x) = \cosh\left(\sqrt{w_{non}}x\right) - \cos\left(\sqrt{w_{non}}x\right) - \sigma_n\left[\sinh\left(\sqrt{w_{non}}x\right) - \sin\left(\sqrt{w_{non}}x\right)\right] \quad (7)$$

Where $w_{non} = (\beta l)^2 = \sqrt{\frac{\rho A l^4}{EI}}w$, where *w* is the corresponding natural frequency of the mode. ρ is the density , A is the cross sectional area of beam, l is the length of the beam, E is the young's modulus while I is the moment of inertia.

b. Contact Regime

We assume only one mode for our beam model, $w_{non} = 3.51602$ and $\sigma_n = .7341$. However, during bouncing we assume a different set of boundary conditions. We assume the last boundary condition to be a spring. Figure (11) shows the boundary conditions present during bouncing.

Figure 11: Beam model representation for contact mode

The boundary conditions are taken from the above figure. The first three boundary conditions remain the same as in the case of the cantilever beam. The last boundary condition is changed to account for the spring at the tip of the beam.

$$\phi(0)=0 \qquad \phi'(0)=0 \qquad \phi''(l)=0 \qquad \phi'''(l)- R_t\phi(l)=0 \tag{8}$$

The last condition equates the shear force of the beam to the spring force from the spring, namely R_t , and it is defined as,

$$R_t = \frac{kl^3}{EI} \tag{9}$$

Using the above boundary conditions and putting the equation in the matrix form,

$$\begin{bmatrix} 1 & 0 & 1 & 0 \\ 0 & 1 & 0 & 1 \\ -\cos(\beta l) & -\sin(\beta x) & \cosh(\beta l) & \sinh(\beta l) \\ (\beta l)^3\sin(\beta l) - R_t\cos\beta l & -(\beta l)^3\cos(\beta l) - R_t\sin(\beta l) & (\beta l)^3\sinh(\beta l) - R_t\cosh(\beta l) & (\beta l)^3\cosh(\beta l) - R_t\sinh(\beta l) \end{bmatrix} \begin{bmatrix} A \\ B \\ C \\ D \end{bmatrix} = \begin{bmatrix} 0 \\ 0 \\ 0 \\ 0 \end{bmatrix} \tag{10}$$

Assuming non trivial solutions for the derived determinant, we get

$$(\beta l)^3 \sinh(\beta l)^2 - (\beta l)^3 \cosh(\beta l)^2 - (\beta l)^3 \sin(\beta l)^2 - (\beta l)^3 \cos(\beta l)^2 + 2R_t \cos(\beta l) \sin(\beta l) - 2R_t \cosh(\beta l) \sin(\beta l) - 2(\beta l)^3 \cos(\beta l) \cosh(\beta l) = 0 \quad (11)$$

From the equation(9), we see that R_t is dependent on the value of the pad stiffness. The stiffness is calculated using the formula $K = \frac{8EI}{l^3}$ for the case of cantilever beams. The pad stiffness is assumed to be 30 times the tip stiffness used [1]. After calculating R_t, βl is calculated and found to be 3.805 for $R_t = 260$.

To calculate the values of the constants in the function $\phi(x)$, we use the above equations to express all the variables in terms of one constant (assuming infinite solutions). The final form for such simplification can be presented as follows,

$$\phi(x) = A\left[\cos(\beta x) - \left[\frac{\cos\beta l + \cosh\beta l}{\sin\beta l + \sinh\beta l}\right]\sin(\beta x) - \cosh\beta(x) + \left[\frac{\cos\beta l + \cosh\beta l}{\sin\beta l + \sinh\beta l}\right]\sinh(\beta x)\right] \quad (12)$$

Using the condition $\int_0^1 \phi^2(x)dx = 1$, which is the result derived from the orthogonality of mode shapes, we can find the value of A which will satisfy all of the homogenous and non-homogenous boundary conditions. The value of A for the first mode shape is found to be 0.87974.

To obtain the 2nd order ODE which will be used to solve for the dynamics of the system, we simultaneously solve the system for the 2 different models, namely the contact model and the free model.

3.1.2 Reduced-Order Modeling

To solve for the dynamical system, we start from the equation (1). We use the Galerkin method to derive the reduced order model by using the beams linear orthonormal mode shapes. We then multiply the equation by the mode shape and integrate it over 1 to 0. The derivation is shown by the equations (13-17).

$$EIw'''' + c\dot{w} + \rho bh\ddot{w} = \frac{\varepsilon b\left[V_{dc}^2\right]}{2(d-w)^2} \tag{13}$$

Where ε is the permittivity of free space and other symbols are same as before.

The equation is nondimensionalised by:

$$\hat{w} = \frac{w}{d}, \qquad \hat{x} = \frac{x}{l}, \qquad \hat{t} = \frac{t}{T} \tag{14}$$

w is the defection, d is the gap between the tip and the substrate, x is the longitudinal coordinate of the beam , l is the total length of the beam and t is the time. $\hat{w}$, $\hat{x}$ and $\hat{t}$ are nondimensionlised deflection, length and time respectively. T is defined as,

$$T = \sqrt{\frac{\rho b h l^4}{EI}}$$

(15)

We substitute equation (2) in equation (13), and replace w to obtain

$$\ddot{u} + w_{non}{}^2 u + c_{non}\dot{u} = \alpha_2 [V_{dc}]^2 \int_0^1 \left\{\frac{\phi}{(1-u\phi)^2}\right\} dx$$

(16)

Where ϕ is the corresponding mode shape and u is the modal coordinate variable. $(1-u\phi)^2$ in the denominator can be tackled in one to two ways. It can be expanded using the Taylor series but such an expansion will require upto 20 terms (12). Or we can multiply both sides by $(1-u\phi)^2$ and ϕ and use the orthonormality of the mode shapes to simplify the system without the need to expand up to 20 terms in the denominator. Implementing the second method, we obtain

$$(\ddot{u} + w_{non}{}^2 u + c_{non}\dot{u})(1 - 2u\int_0^1 \phi^3 dx + u^2 \int_0^1 \phi^4 dx)\alpha_2 \left[V_{dc}^2 + V_{ac}\cos(\Omega t)\right]^2 \int_0^1 \phi dx$$

(17)

3.1.3 Damping Considerations (Squeeze Film Damping)

Near the micro scale, it has been shown that squeeze film damping becomes a dominant mode of damping and hence cannot be ignored if accurate models of bouncing are desired [12]. For accurate simulation we need to solve the equation of motion of the beam coupled with the Reynolds equation using finite element

method or perturbation equations. However the equations can be simplified if we assume the incompressible gas flow model for air [12].

$$c = \frac{b^3 \mu}{[d - w(x,t)]^3} \tag{18}$$

Where *b* is the width of the beam μ represents the viscosity of air and *c* is damping coefficient.

To account for this change, we revise the equation (13). The overall form of the equation is,

$$-\frac{EI\,\partial^4 w}{\partial x^4} - m\frac{\partial^2 w}{\partial t^2} = F_{electrostatic} - F_{SQFD} \tag{19}$$

After normalization we have

$$\frac{\partial^4 w}{\partial x^4} + \frac{\partial^2 w}{\partial t^2} = \frac{\alpha_2 V_{dc}^2}{\left(1 - w(x,t)\right)^2} - \frac{c_{non}}{\left(1 - w(x,t)\right)^3}\frac{\partial w}{\partial t} \tag{20}$$

Where $\alpha_2 = \frac{6\varepsilon l^4}{Eh^3 d^3}$ and $c_{non} = \frac{12cl^4}{ETbh^3}$. The parameters remain same as defined earlier. As before, we assume the *w(x,t)* to be a separable function defined in *u(t)* and $\phi(x)$. Also we multiply both sides by $\left(1 - w(x,t)\right)^3$, $\phi(x)$ and integrate over the entire length. The final result is of the form,

$$\ddot{u} + uw_{non}^2(-u^3\int \varphi^5 dx + 3u^2\int \varphi^4 dx 3u\int \varphi^3 dx\int \varphi^2 dx) + c_{non}\dot{u}(\int \varphi^2)$$
$$= \alpha_2 V_{dc}^2\left[\int \varphi - u\int \varphi^2\right] \tag{21}$$

Where the A is part containing the integration terms not multiplied by the voltage term,

$$A = (-u^3\int \varphi^5 dx + 3u^2\int \varphi^4 dx - 3u\int \varphi^3 dx + \int \varphi^2 dx) \tag{22}$$

We divide both sides A to simplify the equation to give the form in equation (23),

$$\ddot{u} + uw_{non}^2 + \frac{c_{non}\dot{u}(\int \varphi^2)}{A} = \frac{\alpha_2 V_{dc}^2\left[\int \varphi - u\int \varphi^2\right]}{A} \tag{23}$$

3.1.4 Partial Electrode Modeling

Most RF MEMS switches and other devices normally have partial lower electrode. To account for that in our simulations, the electrostatic force is assumed to be represented by a step function corresponding to the starting and ending dimension of the electrode [12]. The forcing term is updated as given in equation (24),

$$F = \frac{\varepsilon b V_{dc}^2 [u(x - x_1) - u(x - x_2)]}{2(d - w(x,t)^2}$$

(24)

In terms of the beam theory, it means changing the integration limits of φ from x_2 to x_1.Hence for partial electrode , all the terms related to the forcing(electrostatic term) have their limits of integration changed to,

$$\int_{x_1}^{x_2} \varphi^N(x)$$

(25)

3.1.5 Double Electrode

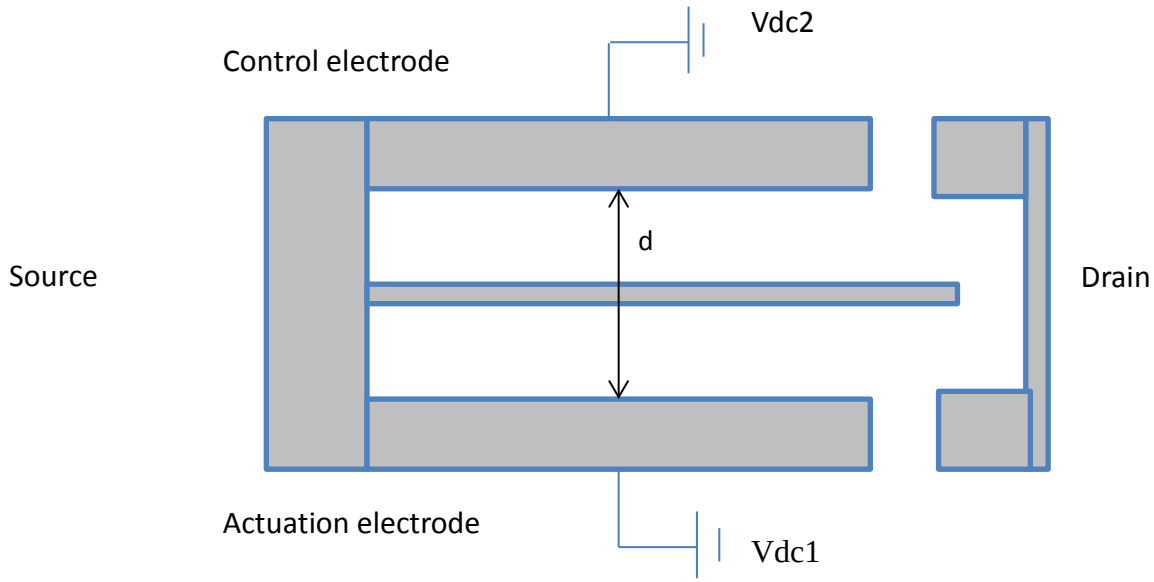

Figure 12: Simplified double electrode model

For the double electrode model, the major change is a new forcing term in the form of the secondary electrode voltage. Here $V_{acutation}$ is the actuation voltage

while $V_{vontrol}$ is the voltage of the second electrode or the control voltage. *w* and *d* are the deflection and the gap between the tip and the substrate respectively. The new electrostatic forcing is,

$$F_e = \frac{V_{actuation}^2}{\left(d - w(x,t)\right)^2} - \frac{V_{control}^2}{\left(d + w(x,t)\right)^2} \tag{26}$$

The overall equation (after normalization) comes in this form,

$$\frac{\partial^4 w}{\partial x^4} + \frac{\partial^2 w}{\partial t^2} = \alpha_2 \left(\frac{V_{actuation}^2}{\left(1 - w(x,t)\right)^2} - \frac{V_{control}^2}{\left(1 + w(x,t)\right)^2} \right) - \frac{c_{non}}{\left(1 - w(x,t)\right)^3} \frac{\partial w}{\partial t} \tag{27}$$

As before, to avoid extensive Taylor series in the denominator we multiply both sides by $(1 + w)^2(1 - w)^3$, which is the common denominator of all terms on the right hand side of equation (27). We use the separation of variables from equation (2) and multiple both side by ϕ (the first mode shape, using same methodology as used in derivation from equation (20)).The final expansion is given in two parts below.

The left hand side of equation (27) expands to

$$\ddot{u} + w_{non}^2 u \left(-u^5 \int \varphi^{7} dx + u^4 \int \varphi^6 dx + 2u^3 \int \varphi^5 dx - 2u^2 \int \varphi^4 dx - u \int \varphi^3 dx \right.$$

$$\left. + \int \varphi^2 dx \right) + c_{non} \dot{u} \left(\int \varphi^2 + 2u\varphi^3 + u^2\varphi^4 dx \right)$$

(28)

The right hand side expands to

$$\alpha_2 \left((V_2^2 - V_1^2) \left(u^3 \int \varphi^4 - \int \varphi \right) - (3V_2^2 + V_1^2) \left(u^2 \int \varphi^3 - u \int \varphi^2 \right) \right)$$

(29)

Same as before, to simplify the equation we collect the integration on the left hand side in one term defined as A,

$$A = \left(-u^5 \int \varphi^{7} dx + u^4 \int \varphi^6 dx + 2u^3 \int \varphi^5 dx - 2u^2 \int \varphi^4 dx - u \int \varphi^3 dx + \int \varphi^2 dx \right)$$

(30)

The final equation can be written in the form

$$\ddot{u} + w_{non}^2 u + c_{non} \dot{u} \frac{(\int \varphi^2 + 2u\varphi^3 + u^2\varphi^4 dx)}{A} = \alpha_2 \frac{\left((V_2^2 - V_1^2) (u^3 \int \varphi^4 - \int \varphi) - (3V_2^2 + V_1^2) (u^2 \int \varphi^3 - u \int \varphi^2) \right)}{A}$$

(31)

3.2 Lumped Mass Parameter model

In the lumped mass model, the entire system is modeled as a spring mass damper system of the form shown in Figure (13). The beam is represented by an effective mass in the lumped mass parameter model. Furthermore an effective

spring constant and a damping coefficient is derived for the system based on the regime as before (contact regime and free regime).

The basic equation implemented in the system is given in equation (27)

$$m\ddot{x} + c\dot{x} + kx = \frac{\varepsilon A[V_{dc} + V_{ac}\cos(\omega t)]^2}{2(d-x)^2} \tag{32}$$

In the equation, m represents mass, while *c* and *k* represents the damping and spring constants respectively. ε is the dielectric constant for vacuum . *A* represents the cross sectional area of the beam and VDC is the DC voltage. *d* is the maximum distance between the beam tip and the substrate.

We drive an equivalent spring mass model with a value of *m*, *c* and *k*. The values of *c* (damping) and *k* (stiffness) change drastically when the contact regime is activated (contact between substrate and tip) and when the free regime is activated (no contact). Both regimes have unique values of *c* and *k* which are derived using 3D models. Figure (13) can be used to visually represent and equivalent spring mass model for both regimes with different values of c and k.

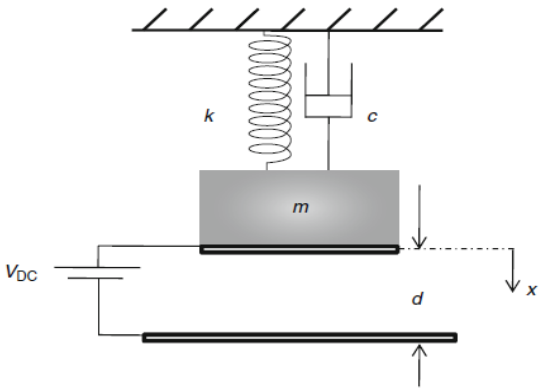

Figure 13: Lumped mass parameter model [12]

3.3 Defining ODE of the System

The dynamics of the system and the bouncing is modeled in two parts using the spring mass damper system, namely the free regime and the contact regime. During the free regime, the beam is not in contact with the substrate hence the resultant spring constant (K) and the damping (C) are much lower. On the other hand, when beam tip touches the substrate (or the dielectric as in our case), the magnitude of C and K becomes higher .We define this regime as the contact regime. In the case of the free regime, the equation of motion is defined as,

$$m\ddot{x} + c_f\dot{x} + k_f x = \frac{\varepsilon A[V_{dc} + V_{ac}\cos(\omega t)]^2}{2(d-x)^2} \tag{33}$$

Where f signifies that the system is in the free regime and hence no contact has occurred. The values for c_f and k_f are taken from simulations.

As soon as the system reaches a specified distance, which is the distance of the dielectric layer as in our system, the equation shifts to contact regime. Note that *c* in the subscript means contact here. As before, the values for C and K are from simulations.

$$m\ddot{x} + c_c\dot{x} + k_c x = \frac{\varepsilon A[V_{dc} + V_{ac}\cos(\omega t)]^2}{2(d-x)^2} \tag{34}$$

a) Double Electrode

In the case of double electrode model, we add a new forcing term to account for the secondary electrode. We assume no change occurs to the beam stiffness and the damping in the system. Hence to account for this change, the forcing term is changed to account for the second electrode,

$$F_e = \left(\frac{Vdc_1^2}{\left(\frac{d}{2} - x\right)^2} - \frac{Vdc_2^2}{\left(\frac{d}{2} + x\right)^2} \right) \tag{35}$$

Other parts of the equation remain the same.

Chapter 4.
Simulations

Several simulations are conducted to model the effect of bouncing accurately. The final purpose of the simulation is to show that the bounce may be reduced by implementation of open loop control in the form of pulse shaping functions. Since accurate simulations required changing ODE mid simulations, Simulink is chosen as the main program due to its excellent support for dynamical system simulations and modeling.

4.1 Results of the Lumped Mass Parameter Model

The parameters for the model are taken from [5]. The parameters used for the model are presented in table 1.

Table 1: Parameters for the lumped model [4]

Parameter	Value
Natural frequency free (w_f)	2.1 x 10^4 Hz
Damping free	2 x 10^{-2}
Gap (d)	3.8 x 10-6 m
Maximum distance to travel	2.6 x 10-6 m
K (eA/2m)	1.9 x 10-11 [F.m/kg]
Effective spring constant	42 N/m
Natural frequency contact (w_c)	6.1 x 104Hz
Damping (contact)	2 x 10^{-1}

4.1.1 Bouncing Characteristics Shown Using Uncontrolled Actuation

The equations of motion derived equation (33-35) are numerically integrated in Simulink to obtain the bouncing dynamics. The overall bouncing for the double beam electrode was simulated for the case of 0 control voltage. Figure (14) shows this profile with the corresponding displacement and velocity.

a

b

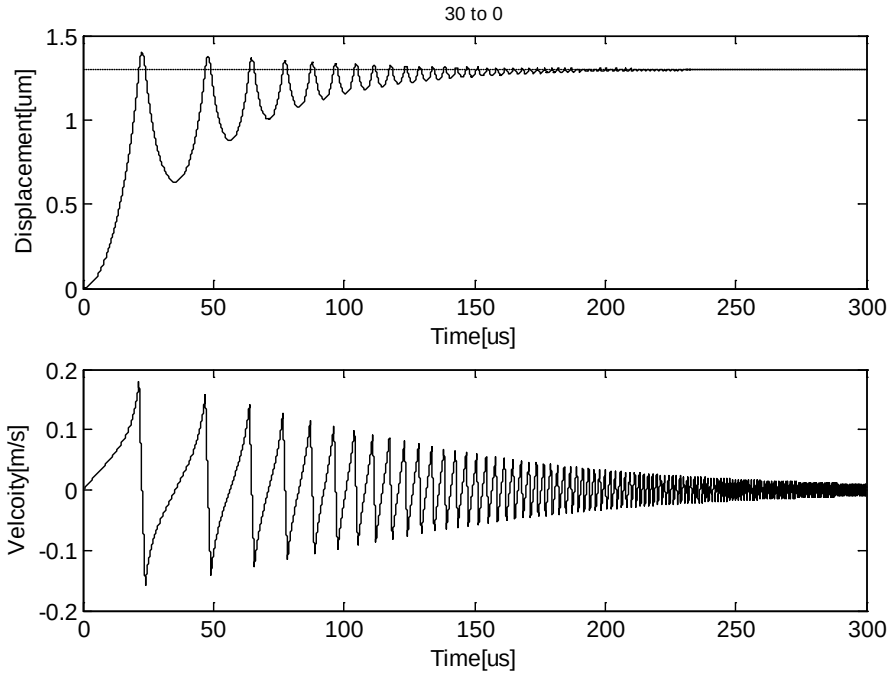

Figure 14: The total bouncing profile part a: Displacement of tip. Part b: velocity

4.1.2 Control of Bouncing Using the Double Electrode

The landing velocity and landing time are the velocity and time respectively of the tip when it reaches the substrate. The average settling time is the average time for amplitude of bounce to reduce to *5%*. Average bounce is the average of first eight displacements of the tip above the substrate (12).

The effects on these parameters are tested by changing several variables. The variables tested are actuation and control pulse interaction, actuation and control voltages, control pulse timing and control pulse shape. Definitions of the variables are provided in their relevant section

a) Single Electrode Uncontrolled Values

For the case of zero control voltage and 30 V actuation voltage, the landing time, landing velocity and other results obtained are shown in table 2.

Table 2: Uncontrolled variable results

Landing time[μs]	Landing velocity[m/s]	Average bounce[μm]	Average settling time[μs]
21.5	0.1784	0.358	13

b) Control of Beam Dynamics by Varying Actuation Voltage and Control Voltage

Voltage control refers to the dependence on landing velocity and the landing time with both actuation and control voltages. Since voltage appears in the forcing term, it directly affects the dynamics of the system. Higher voltage will allow for faster switch closing times but with higher impact velocities. This could be mitigated

by using higher voltages in the control electrode to slow down the beam. Both the effects of control voltage and actuation voltage are studied in this document.

- **Using Control voltage as the Control Parameter**

The dynamics of the switch and all the major parameters are strongly affected by the control voltage and hence it is one of the tools that can be used to reliably optimize the system. Table (4) shows the dependence of control voltage on the landing times and landing velocity. It can be seen that for a control voltage of *9* V, the landing velocity, average settling time and average bounce are reduced by *43%*, *98%* and *102%* respectively, while the landing time increases by *11%*.

Table 3 lists the percentage changes with respect to the uncontrolled actuation for changes in control voltage.

Table 3: Selected percentage changes values from uncontrolled actuation for control voltage for actuation voltage 30V, pulse width 6 μs and pulse timing 17μs

Control Voltage [V]	% Change for landing time	% Change for landing velocity	% Change for Average bounce	% Change for average settling time
1	10.59%	-43.18%	-71.59%	-84.20%
2	10.64%	-43.92%	-88.85%	-94.40%
3	10.64%	-43.66%	-85.20%	-97.24%
7	10.73%	-43.37%	-86.11%	-98.42%
8	10.78%	-43.48%	-79.43%	-90.67%
9	10.82%	-43.48%	-97.83%	-101.90%
10	10.87%	-43.38%	-88.56%	-98.00%
11	10.92%	-43.17%	-80.38%	-88.32%

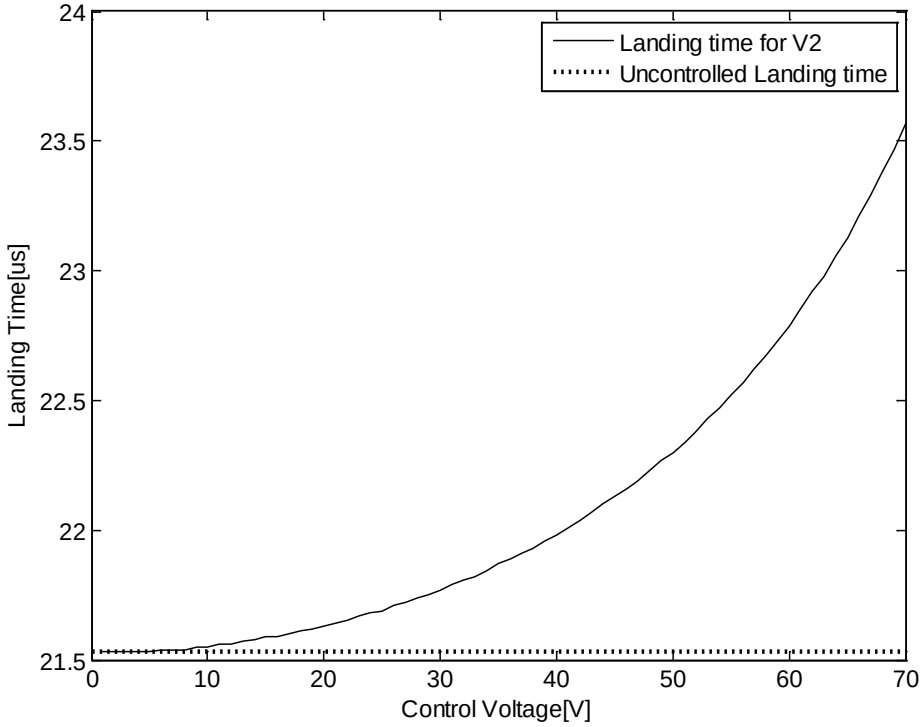

Figure 15: Landing time vs control voltage

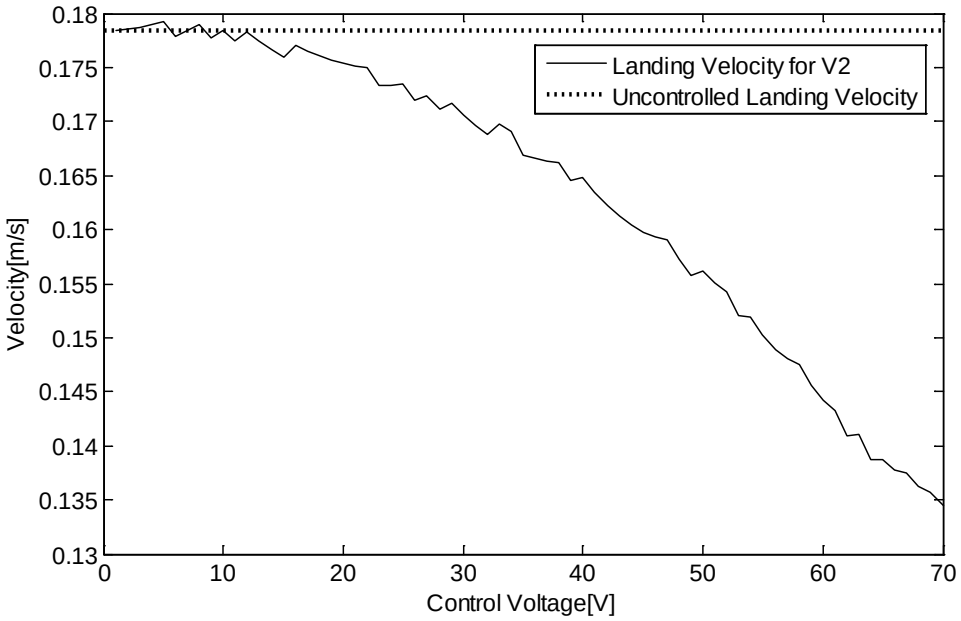

Figure 16: Landing velocity vs control voltage

Overall, the control voltage improves all landing velocity for a minor increase in landing time, However, it improves the average bounce and settling times considerably. Also, the landing time increases and the velocity decreases as control voltage is increased.

- **Using Actuation Voltage as the Control Parameter**

Table 4: Selected percentage change values from uncontrolled actuation for actuation voltage with control voltage at 20V pulse width 6 μs and pulse timing 17μs

Actuation Voltage [V]	% Change for landing time	% Change for landing velocity	% Change for Average bounce	% Change for average settling time
21	86.86%	-42.96%	1.72%	-43.96%
22	73.43%	-39.41%	-62.17%	-77.40%
23	62.01%	-35.38%	-99.92%	-100.00%
24	52.21%	-32.90%	-74.83%	-92.53%
25	43.61%	-30.24%	-45.10%	-62.71%
26	36.04%	-28.97%	-52.33%	-59.83%
27	29.22%	-27.72%	-44.79%	-56.67%
28	23.04%	-28.75%	-63.06%	-74.04%
29	17.28%	-32.35%	-95.77%	-103.76%
30	11.66%	-42.50%	-87.59%	-97.08%

Actuation voltage strongly influences both landing time and velocity. From the table 4 and figures 17 and 18, we see that actuation voltage may be used to

reduce landing time by sacrificing device performance in velocity, settling time and average bouncing.

There is a local minimum observed in the system, figure (18). This will be discussed thoroughly in the section 4.1.2 d .

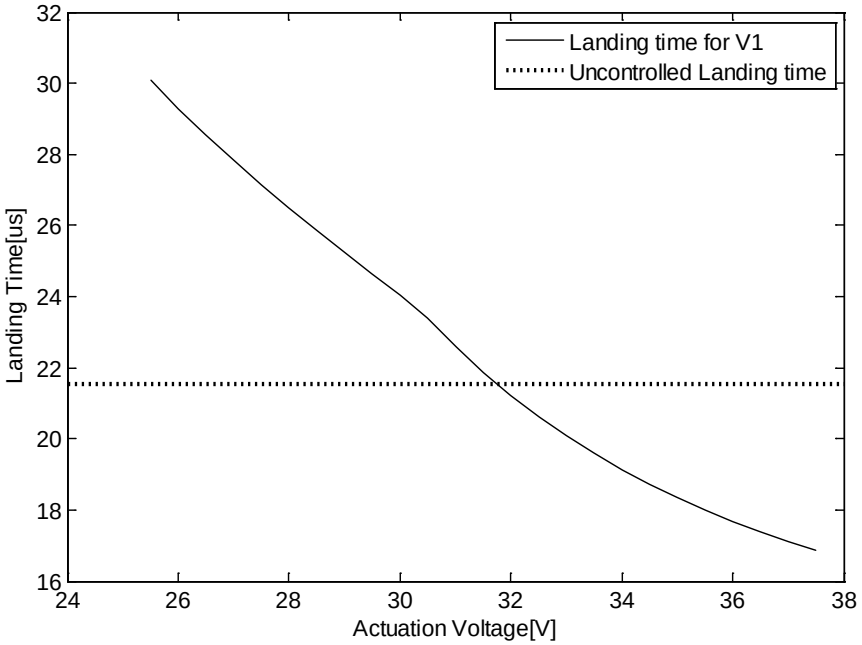

Figure 17: Landing time vs actuation voltage

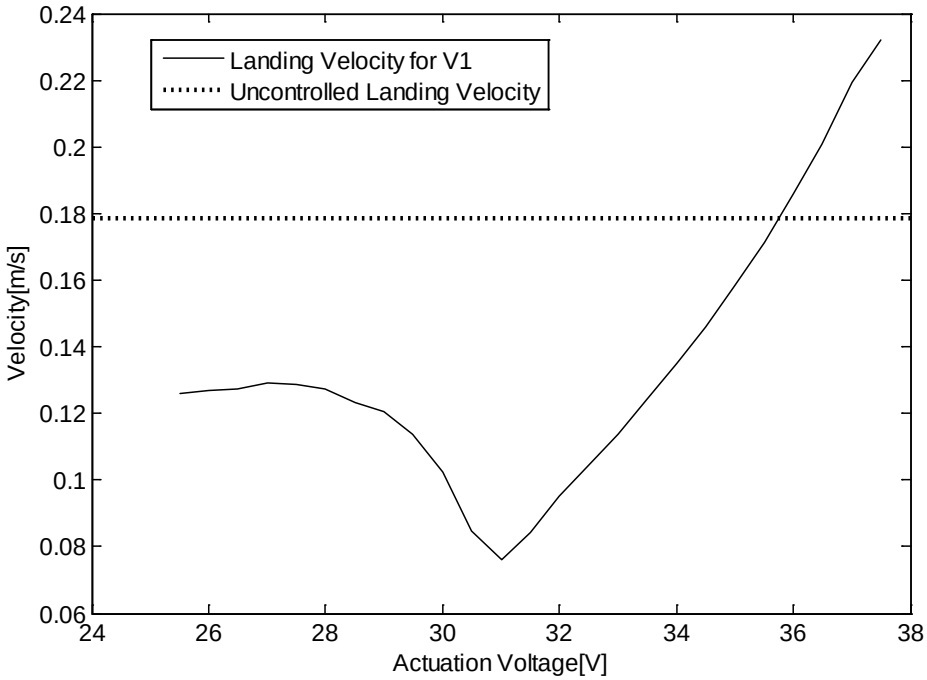

Figure 18: Landing velocity vs actuation voltage

c) Using Different Control Pulse applications as Control Parameter

We determine the change in the dynamics of the system by applying the actuation voltage continuously or applying it only when the control voltage is off.

- **Non Continuous Application of Actuation Voltage**

Figure (19) shows an example of this type of waveform. Table 5 shows the numerical results and graphs obtained for the non-continuous application of actuation voltage in terms of varying pulse width. The effect of pulse width is explained in the section 4.1.2 e.

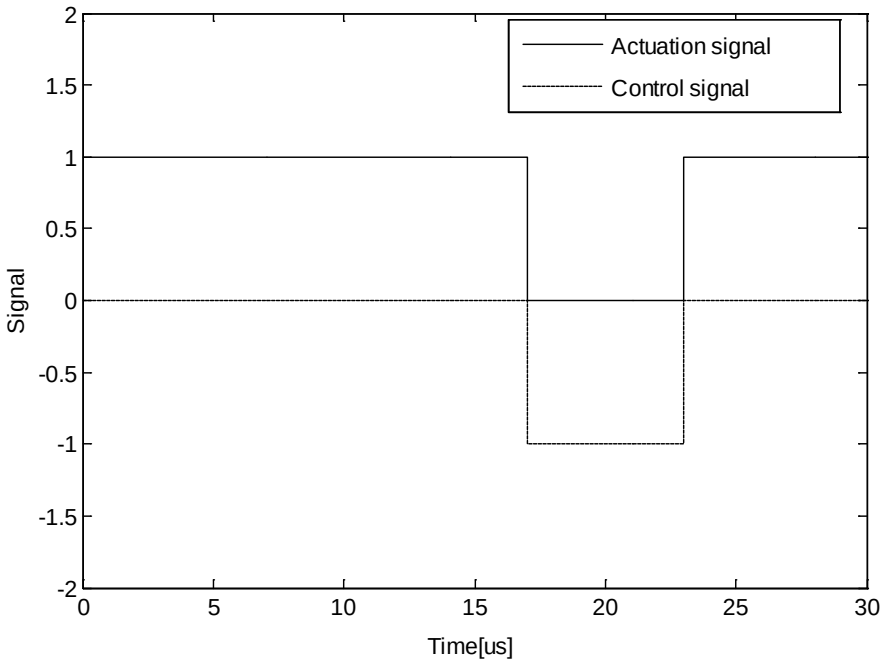

Figure 19: Signal status for non-continuous application of actuation voltage

From table 5 and figures 20 and 21, the tradeoff between the different parameters is seen with respect to uncontrolled actuation. It is seen that a massive reduction in landing velocity, average bounce and average settling time can be achieved by applying non continuous actuation voltage. For one particular case, it is seen that by applying a pulse width of *14 μs*, from *17 μs*, can allow for a reduction in landing velocity for *83%* , both settling time and average bounce are reduced by *100%*.

Table 5: Percentage change from uncontrolled actuation for pulse width-for non-continuous application of actuation voltage with control voltage at 20V actuation voltage at 30V and pulse timing 17μs

Pulse width [μs]	% Change for landing time	% Change for landing velocity	% Change for Average bounce	% Change for average settling time
19	96.24%	-13.82%	-59.78%	-64.39%
18	82.26%	-18.33%	-76.89%	-86.34%
17	69.86%	-26.01%	-57.98%	-69.97%
16	58.71%	-37.33%	-93.78%	-105.47%
15	47.98%	-59.68%	-91.21%	-98.31%
14	24.62%	-82.38%	-99.48%	-100.16%
13	13.33%	-67.64%	-23.33%	-24.30%

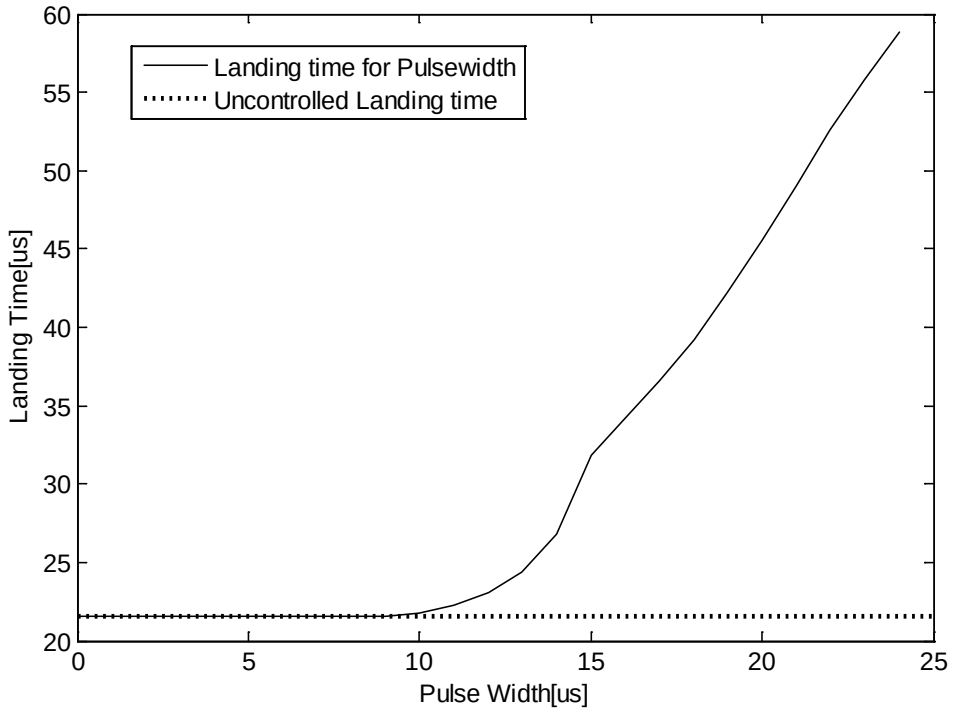

Figure 20: Landing time vs pulse width for non-continuous application of actuation voltage

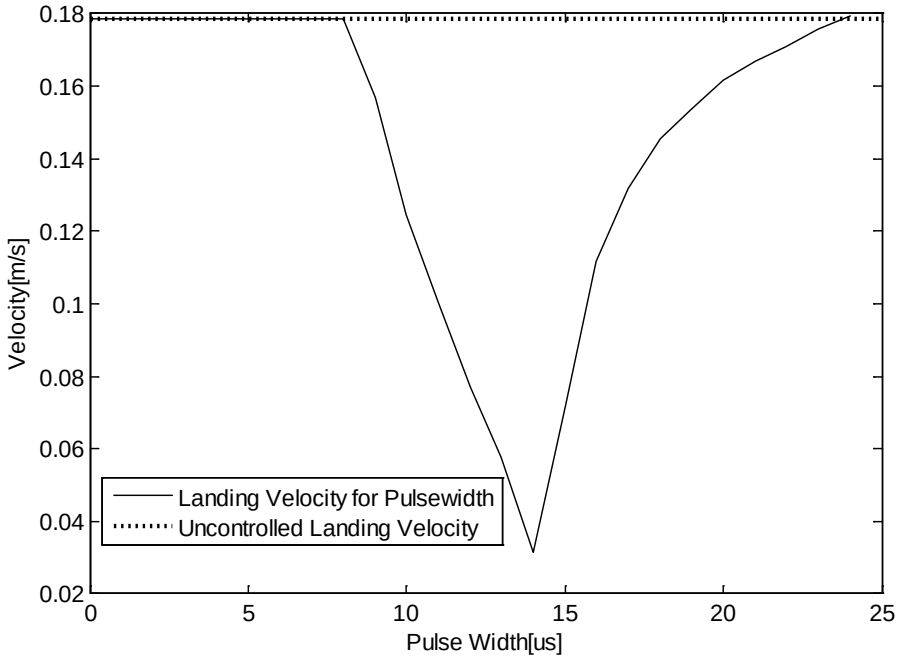

Figure 21: Landing Velocity vs pulse width for non-continuous application of actuation voltage

- **Continuous Application of Actuation Voltage**

Continuous application of actuation voltage implies that actuation voltage is always activated while the control voltage will be turned on for specific time interval. Figure (22) shows an example of this type of waveform. Table 6 and figures 23 and 24 show the results obtained.

From the results, we see that the continuous application of actuation voltage fails to make an impact on reducing landing time and velocity as the reduction is only minimal. For the same pulse width application and other factors, the reduction for velocity is caped below *5%*.

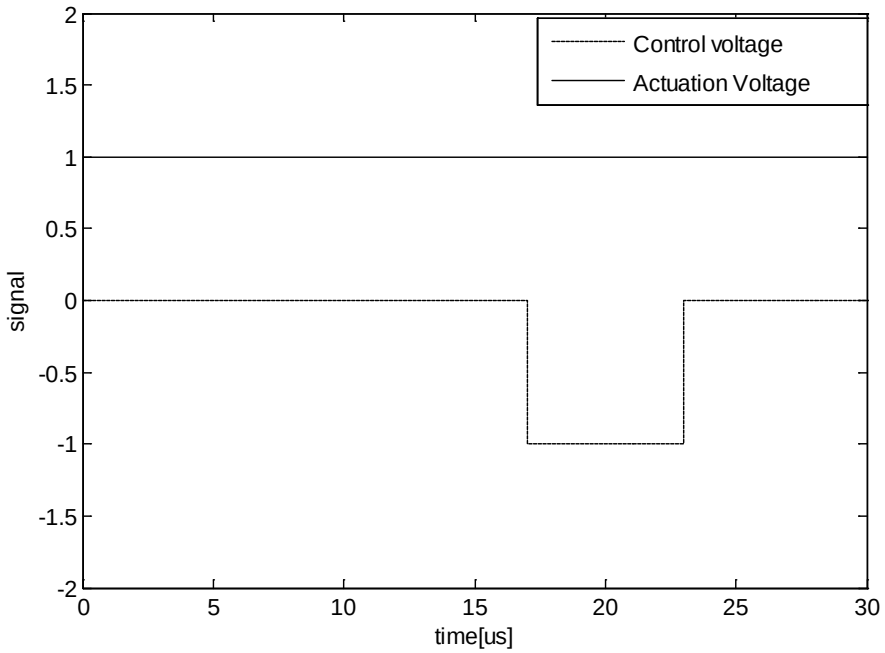

Figure 22: Signal status for continuous application of actuation votlage

Table 6: percentage change in parameters for pulse width--for continuous application of actuation voltage with control voltage at 20V actuation voltage at 30V and pulse timing 17µs

Pulse width [µs]	% Change for landing time	% Change for landing velocity	% Change for Average bounce	% Change for average settling time
19	2.60%	-3.22%	-43.96%	-63.71%
18	1.95%	-2.64%	-24.65%	-27.43%
17	1.44%	-2.45%	-40.37%	-43.51%
16	1.02%	-2.04%	-12.07%	-10.89%
15	0.70%	-1.69%	-22.39%	-24.99%
14	0.46%	-1.70%	1.06%	0.98%

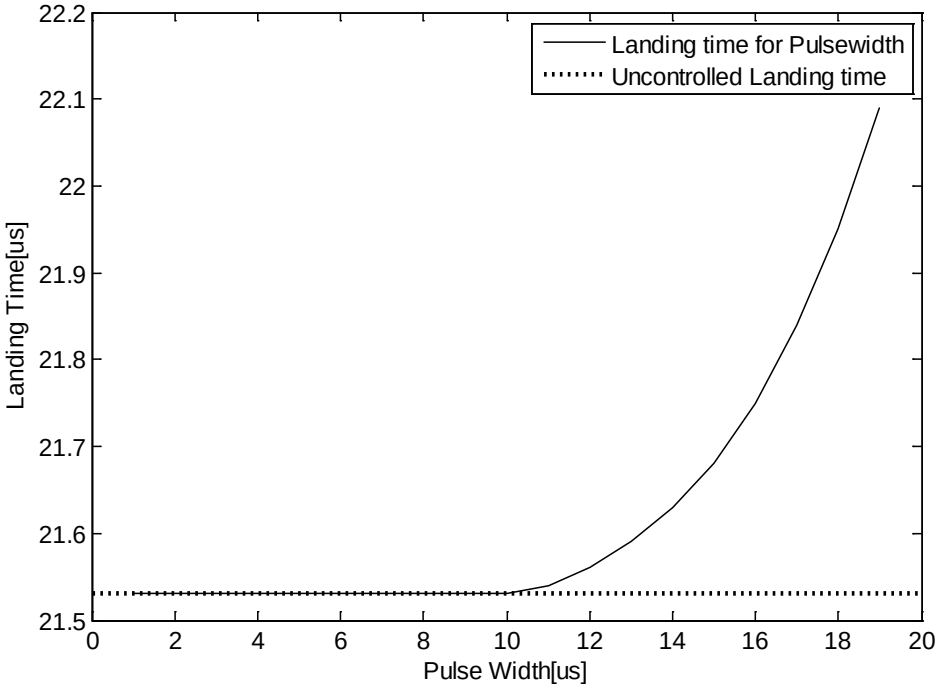

Figure 23: Landing time vs Pulse width

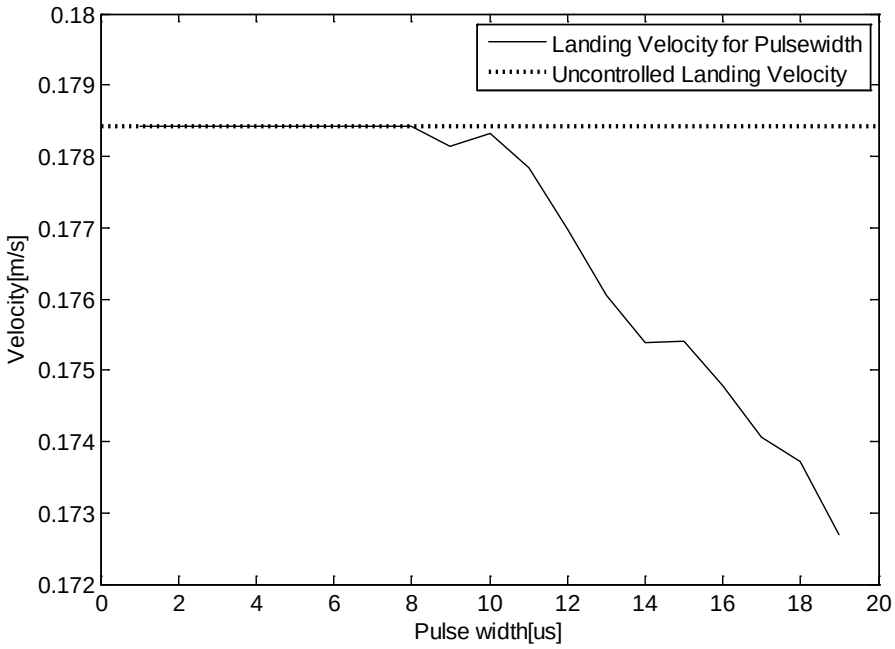

Figure 24: Landing velocity vs pulse width

d) Discussion for Low Velocity Present in Non-Continuous Application of Actuation Voltage

From the figures (20, 21) and (23, 24), it can be seen that for some values of actuation voltage the velocity attains a local minimum. Also, it is observed that non continuous application of actuation voltage allows for a much greater reduction in the landing velocity as opposed to continuous application. This is due to the fact that during certain values of the actuation voltage, the landing time falls completely between the pulse width of the control voltage. This allows for the control voltage to rapidly decelerate the beam in the absence of the actuation voltage and hence reach much lower velocity at landing time. This is the main reason we see a local minimum in the graphs. After the minimum, other values of voltage as in figure (25) give higher landing velocities.

The figure below explains this phenomenon. For high voltages, the landing time occurs before the application of the control pulse hence we see that the pulse does not affect landing time. For the lower voltages, the landing time occurs after the application of the control pulse. This allows the actuation voltage, which dominates the forcing near the beam (see equation 35), to reaccelerate the beam and give higher landing velocity. The best result occurs when the landing time happens at the end of the control pulse width allowing for maximum deceleration of the beam.

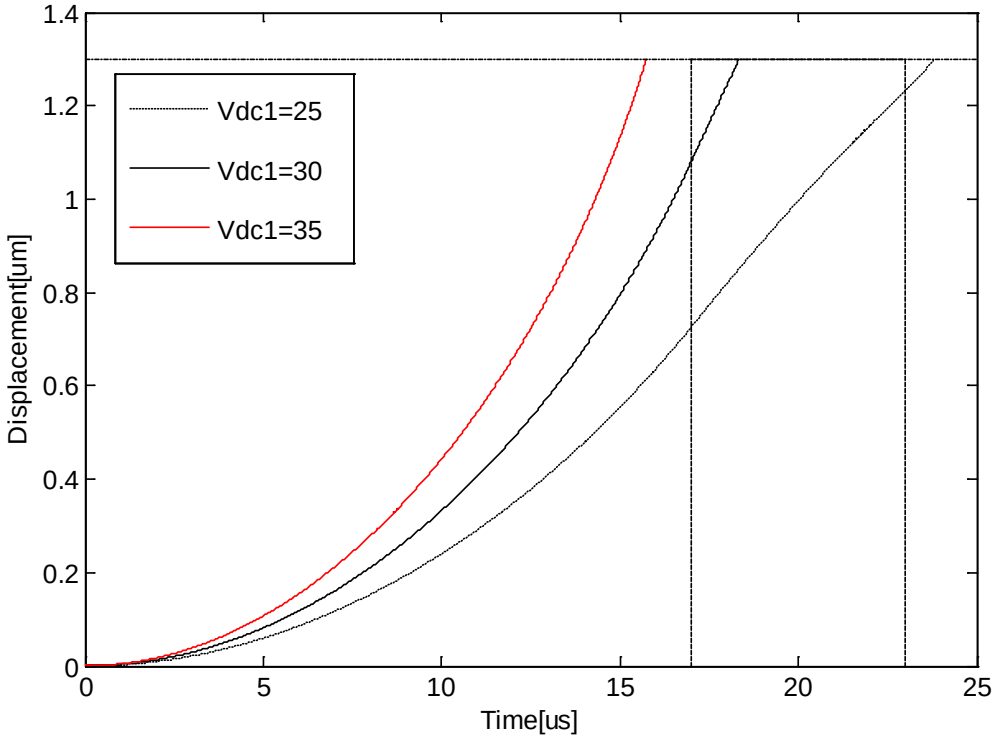

Figure 25: Landing times for different actuation voltages

e) Control Pulse Width

Control pulse width is defined as the total time duration the pulse has been active. Pulse width does not include any preference for starting or ending time and is only the difference between the two starting and ending time of the control pulse. Control pulse width has been identified as a possible variable for minimizing bouncing. Since the system is nonlinear, it is hard to pin point the optimized pulse width that will minimize both landing velocity and time and hence bouncing. Several simulations were done on the aforementioned switch to choose the most effective pulse width. For the above cases presented in figures (20-24), it can be seen that

changing the pulse width directly effects both landing times and velocity. Taking the non-continuous application of actuation voltage for reference (see figure 21), we see that as the pulse width decreases the landing velocity substantially, while increasing the landing time.

f) Control Pulse Timing

Control pulse timing is defined as the time the control pulse is first applied. Pulse timing has been found to be one of the most important parameters in reducing bouncing. Since application of the control pulse only affects the dynamics of the system if applied before the initial contact between the tip and the substrate. The table 7 and figures (26-27) show the effect of increase pulse timing on the dynamics of the system.

As seen from the graphs and table 7, correct application of the pulse before the first impact can significantly reduce bouncing as well as subsequently change the landing time and velocity of impact for later time periods. Too late application of the pulse will prevent any meaningful control as can be seen in the latter half of both figure (26) and figure (27).

Table 7: Percentage change from uncontrolled actuation for pulse position/pulse timing with control voltage at 20V actuation voltage at 30V and pulse width at 14μs

Pulse position [µs]	% Change for landing time	% Change for landing velocity	% Change for Average bounce	% Change for average settling time
11	2.60%	-3.22%	-16.27%	-20.34%
12	1.95%	-2.64%	-5.74%	-6.42%
13	1.44%	-2.45%	-3.97%	-4.46%
14	1.02%	-2.04%	-21.96%	-30.07%
15	0.70%	-1.69%	-42.36%	-62.16%
16	0.46%	-1.70%	1.06%	0.98%
17	0.28%	-1.33%	-88.71%	-113.40%
18	0.14%	-0.81%	-79.49%	-100.84%
19	0.05%	-0.33%	-91.05%	-111.11%
20	0.00%	-0.06%	7.61%	7.70%

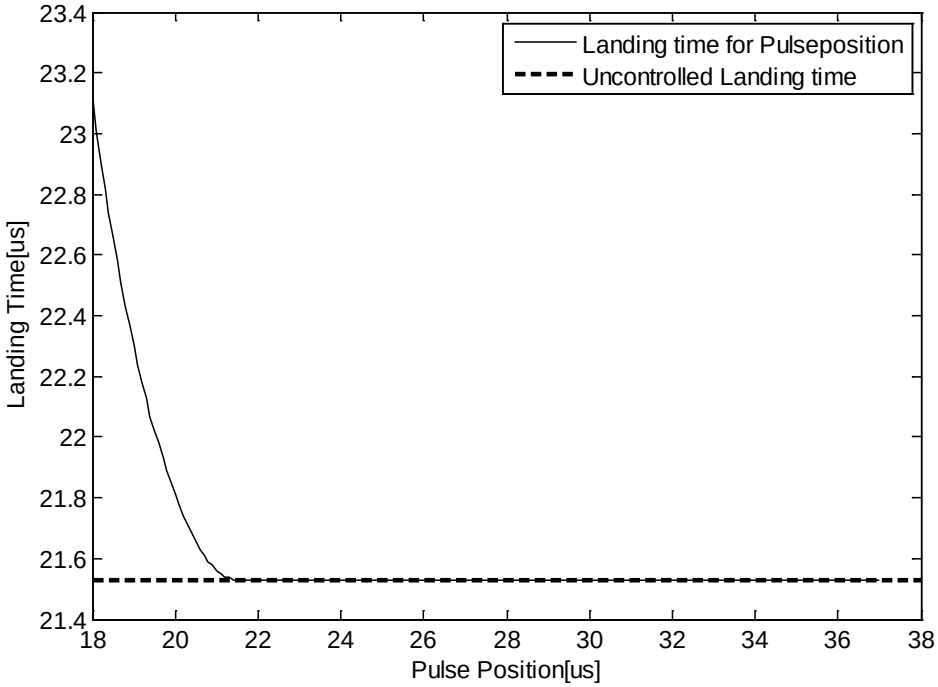

Figure 26: Landing time vs pulse position

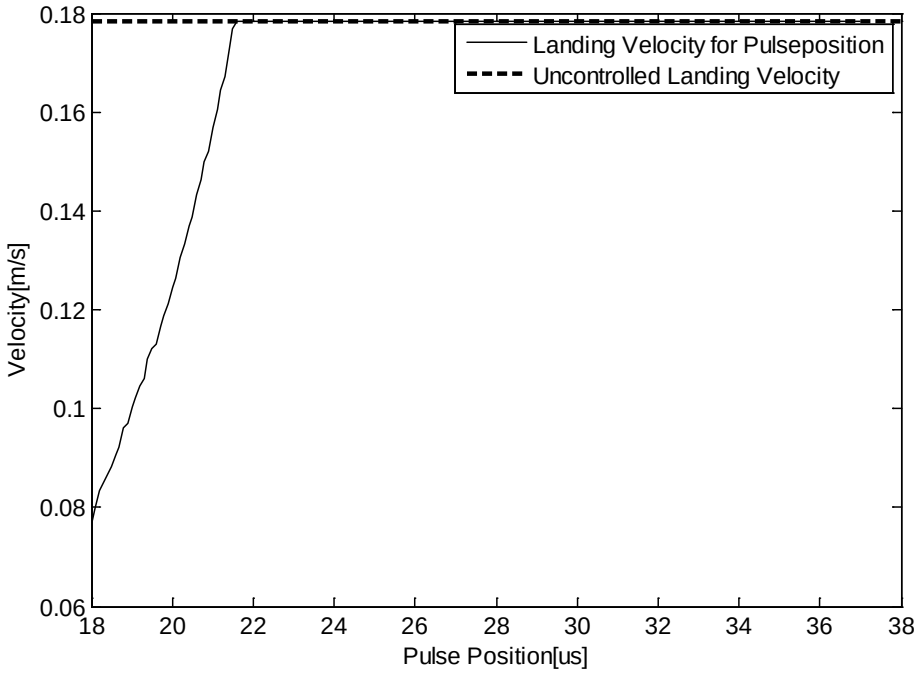

Figure 27: Landing time vs pulse position

g) Control Pulse Shape

Different input functions are used to provide the voltage in a variety of different shapes. AC voltage is a common input source for electrical applications; hence an AC pulse in the form of a sine wave is input to the system and tested. The effect of the control voltage in the form of the AC voltage is shown.

Table 8: Percentage changes from uncontrolled actuation for application of half sine wave with control voltage at 20V pulse width 6 μs and pulse timing 17μs

Control voltage[V]	% Change for landing time	% Change for landing velocity	% Change for Average bounce	% Change for average settling time
21	86.86%	-42.96%	1.72%	-43.96%
22	73.43%	-39.41%	-62.17%	-77.40%
23	62.01%	-35.38%	-99.92%	-100.0%
24	52.21%	-32.90%	-74.83%	-92.53%
25	43.61%	-30.24%	-45.10%	-62.71%
26	36.04%	-28.97%	-52.33%	-59.83%
27	29.22%	-27.72%	-44.79%	-56.67%
28	23.04%	-28.75%	-63.06%	-74.04%

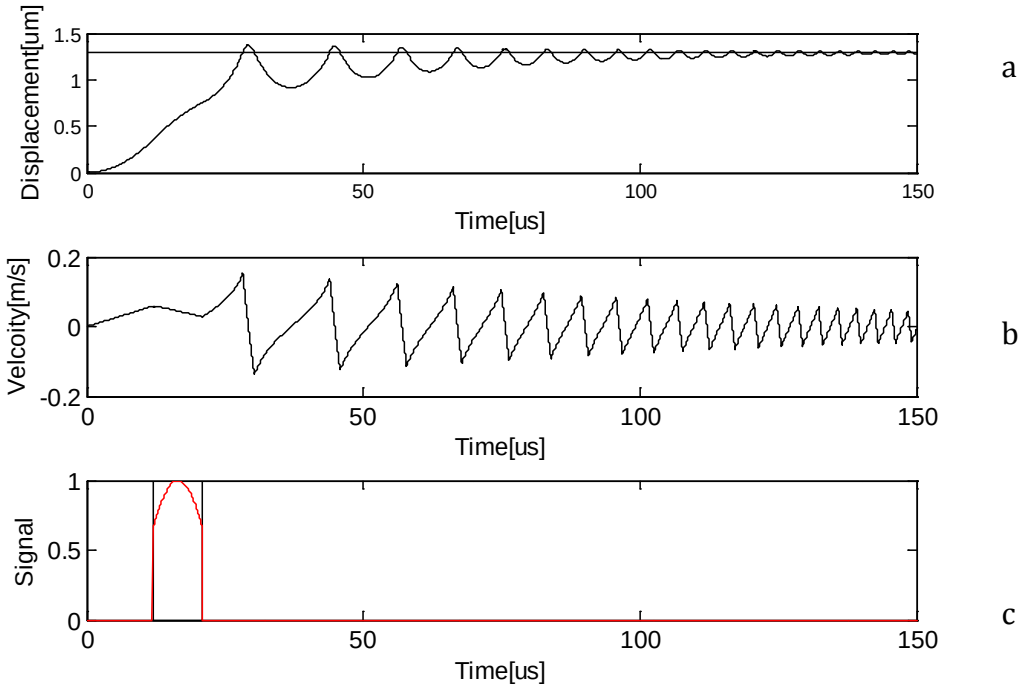

Figure 28: The total bouncing profile part a: Displacement of tip. Part b: velocity profile and part c: signal shapes. Red signal signifies control voltage and the black signal shows actuation voltage

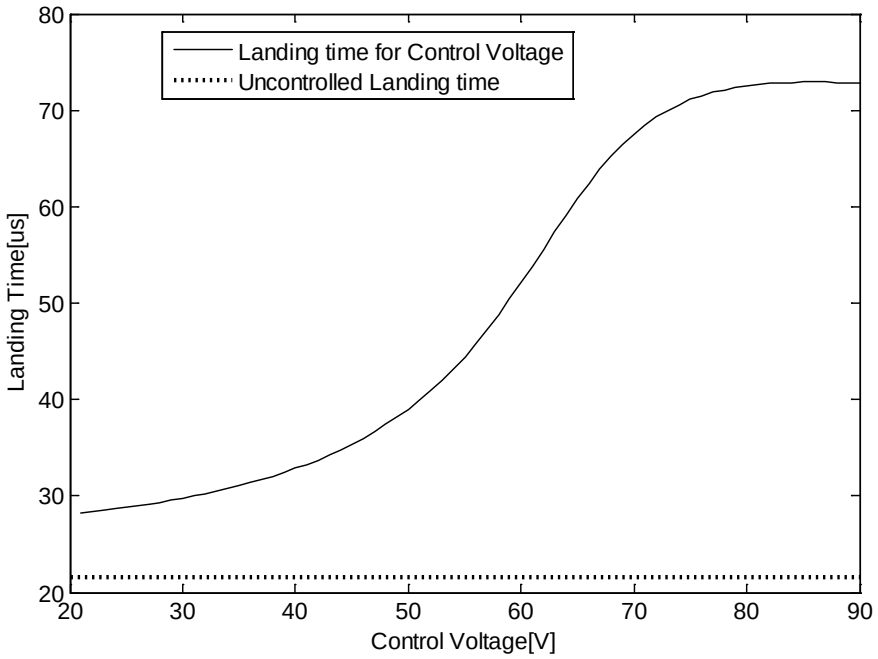

Figure 29: Landing time vs Control Voltage

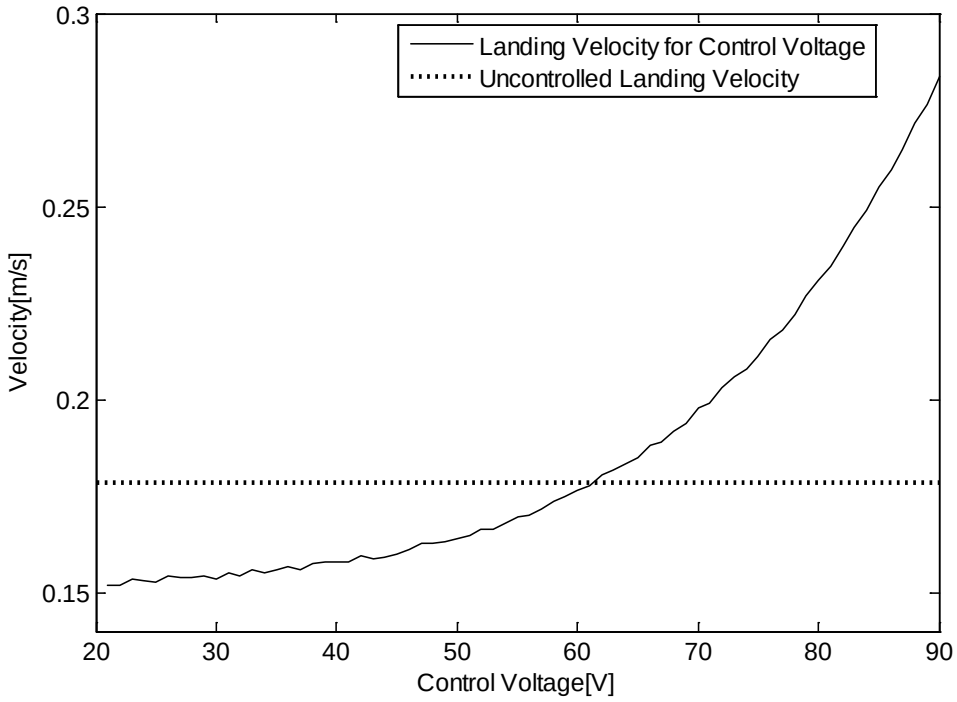

Figure 30: Landing velocity vs control voltage

The result is similar to the control square wave case. The square wave provides better dynamics compared to the AC wave. However since it is hard getting perfect square waves in real life simulations, the half sine wave may provide a more accurate model for real life testing.

4.1.3 Tuning for Zero Landing Velocity

Tuning the entire system that includes damping effect can be quite difficult since the equation representing the system does not have an analytical solution. However, there are certain best practices that may be followed to provide an optimized result. As damping has a minor role to play in the overall dynamics of the

system compared to the other parameters, for the sake of simplicity, we ignore damping in this analysis.

The overall idea of this tuning is to ensure the tip has zero kinetic energy when it touches the substrate. As the switch moves closer to the substrate, more and more energy is stored as elastic energy in the beam. The only source of energy is the voltage in the form of the actuation voltage. The basic idea is to dissipate all the energy not stored as elastic energy, using the control voltage.

Figure 31 shows a sample application of the pulse with the tuning method discussed. Note that the actuation voltage is applied from 0 to t_a while the control voltage is applied from t_a to t_l. Also, d_g is the distance to the substrate while x_a is the distance at which the control voltage is first applied.

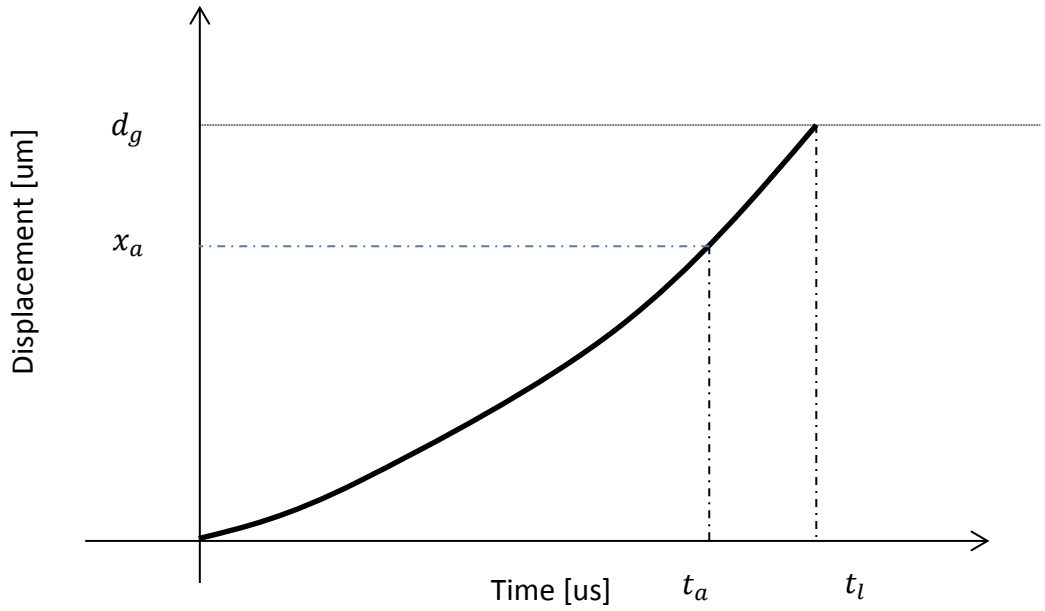

Figure 31: Application of the control pulse.

The first parameter that needs to be experimentally determined is the landing time of the switch. After that, the application of the control pulse has to be fixed in such a way that it includes the landing time of the switch. A good practice is to set the ending time of the control pulse width equal to the landing time. The starting time of the control pulse width can be set according to user requirements (such as 40% of landing time). This will ensure that the landing time will occur during the application of the control voltage to provide minimum landing velocity.

One of the major problems of this method is obtaining x_a, the beam tip distance travelled at the time the control pulse is applied. As, the governing equation of motion is strongly nonlinear, there is no analytical solution to the ODE forcing us to use numerical methods to obtain x_a. After acquiring x_a , it is easier to obtain the other parameters as they can directly be derived using the pulse width and beam parameters (see figure 31) . As stated earlier, our objective is to achieve zero kinetic energy during the landing time, hence we equate the total energy terms present in the system.

$$Energy = \int_0^t F_{electrostatic} \, . \, v \, dt \tag{43}$$

As $vdt = dx$

$$Energy = \int_0^x F_{electrostatic} \, . \, dx$$

(44)

Hence equating the energy terms,

$$\text{Energy provided by actuation voltage} - \text{Stored eleastic energy} = \text{Energy dessipated by control voltage}$$

(45)

$$\int_0^{x_a} \left(\frac{V_{dc1}}{2(d-x)^2}\right) dx - \frac{kd_g^2}{2} = \int_{x_a}^{d_g} \left(\frac{V_{dc2}}{2(d+x)^2}\right) dx$$

(46)

Solving the above equation for the control voltage can provide an optimized system that will provide close to zero landing velocity.

Figure (32) shows a final tuned figure with zero bouncing. Using the earlier method, it is possible to find parameters in close proximity to the optimized parameters that will allow soft landing.

Tuning allowed reducing the bouncing considerably as well as reducing the landing velocity of *9cm/s*. This may be repeated with other pulse shapes and beams of different dimensions to obtain landing with virtually no bounce. However, it can be seen that the landing time has increased *24 us* to *31us*.

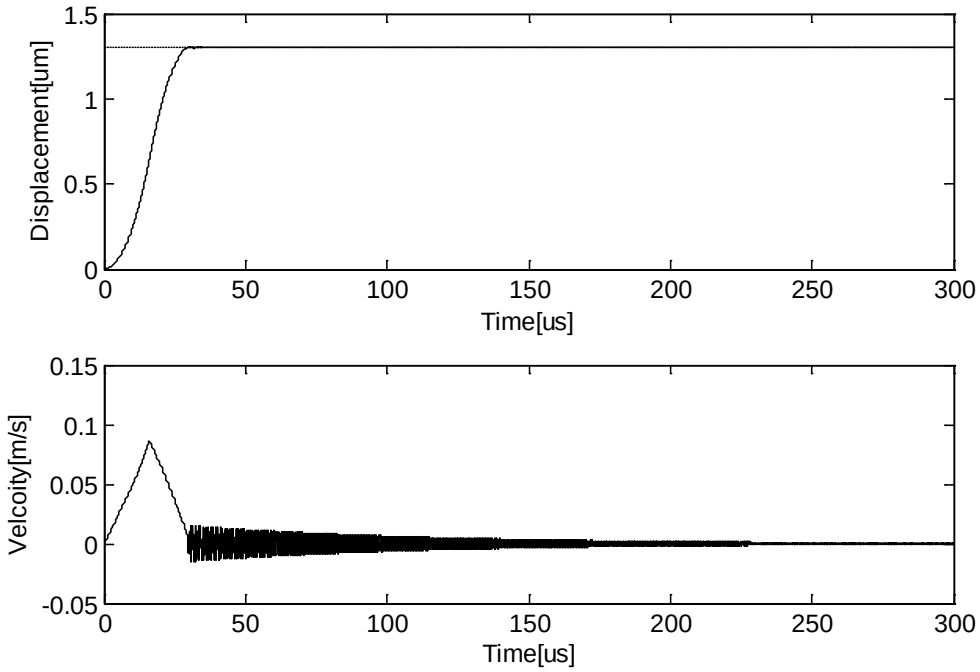

Figure 32: Final tuned figure with displacement and velocity profiles

4.1.4 Comparison with literature

To compare the efficiency of the double electrode model, we simulate the ability of the control technique to reduce landing time and velocity. As such two different types of actuation waves in the literature were compared. Dual Pulse actuation waveform (DP) and exponentially increasing dual pulse waveform (EDP) were simulated based on [13] and tested with similar parameters against the double electrode scheme. Dual pulse actuation waveform consists of an actuation phase followed by a holding voltage. While the EDP has a similar shape with the difference being the initial actuation is achieved through exponentially increasing voltage. The general shape waves are given in Figure (33). To compare these waveforms for the

case of double electrode model, we modify the waveforms with the inclusion of a control voltage (V_c). The figure below presents the general shape of the tested waves. Table 9 shows the values used to compare the two waveforms.

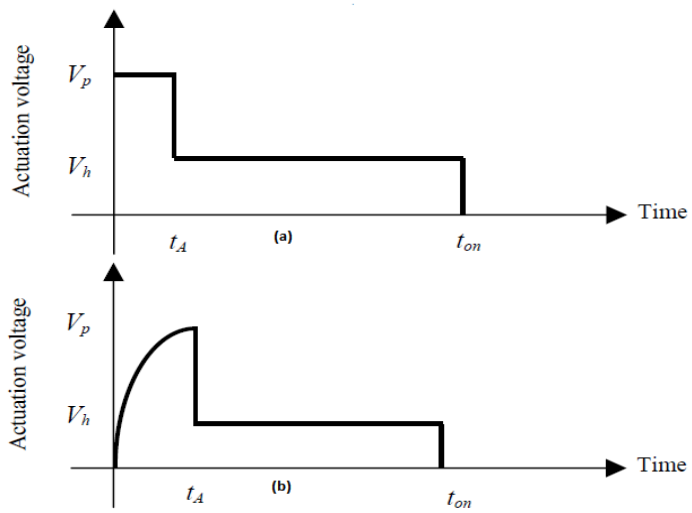

Figure 33: Dual pulse actuation waveform and exponentially increase dual pulse actuation waveform[13]

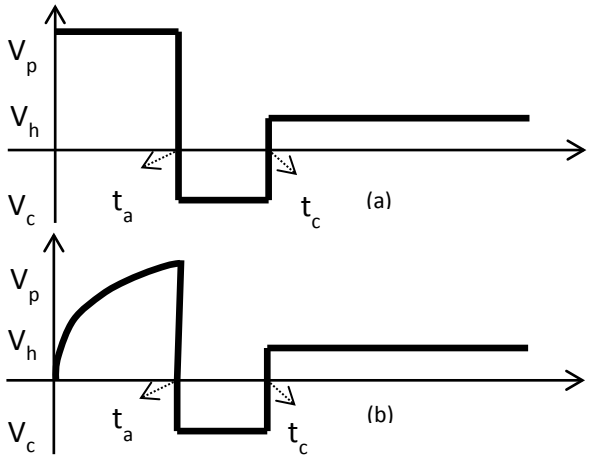

Figure 34: DP and EDP waveforms used for our double electrode model

Table 9: Literature compares parameters for different waves

	ta [us]	Vp[V]	Vh[V]	Vc[V]	t_C[us]
DP	17.4	80	40	-	-
DP Double electrode	17.4	85	40	53.1	19.9
EDP	26.4	80	40	-	-
EDP Double electrode	29	80	40	50	31.405

Using data from table 9, the displacement and velocity profiles are obtained given in figure (35) and figure (36).

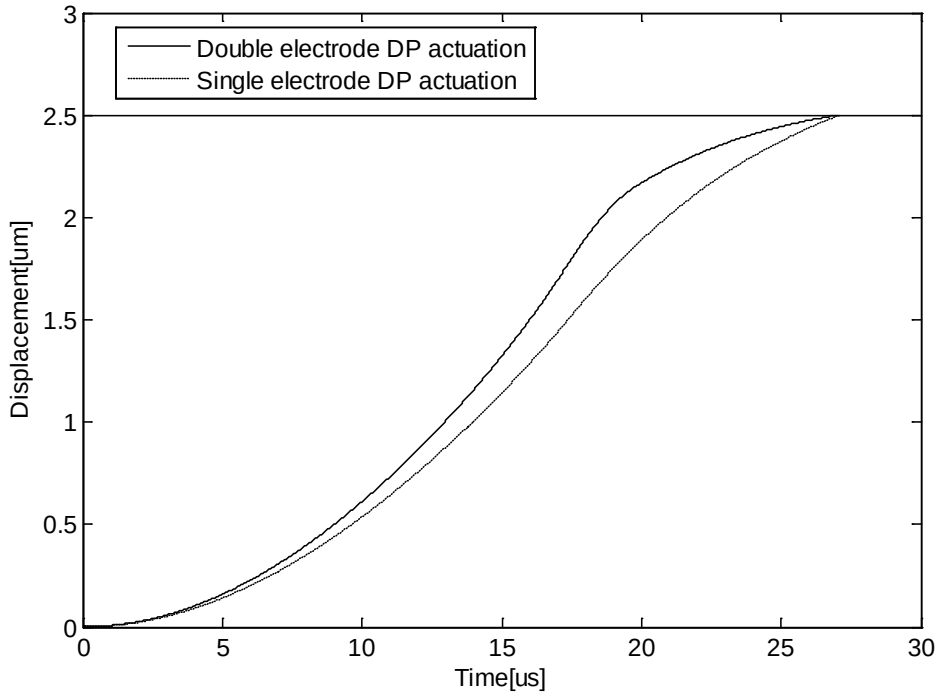

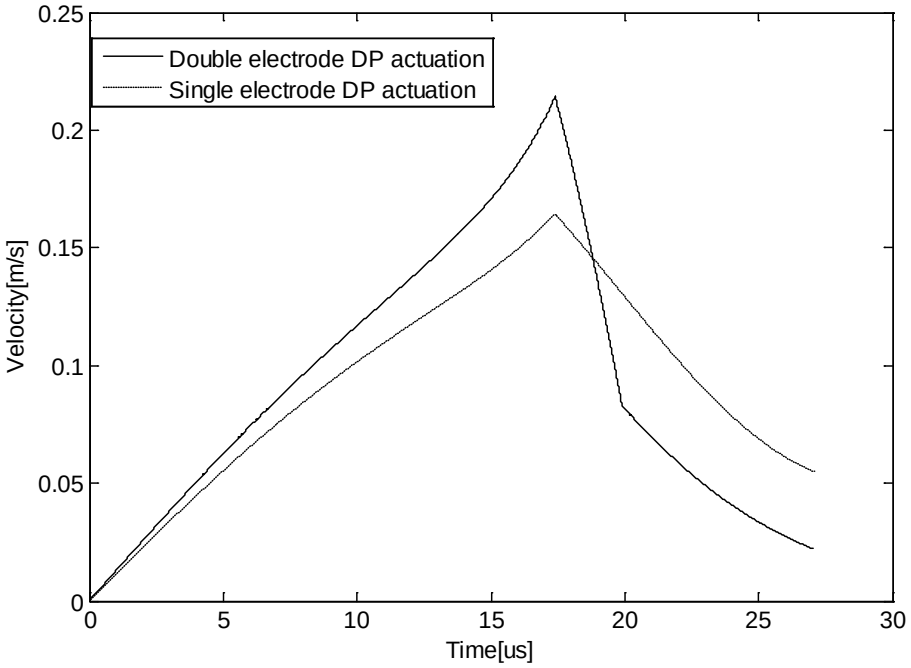

Figure 35: Landing time and landing velocity comparison between DP and DP using double electrode

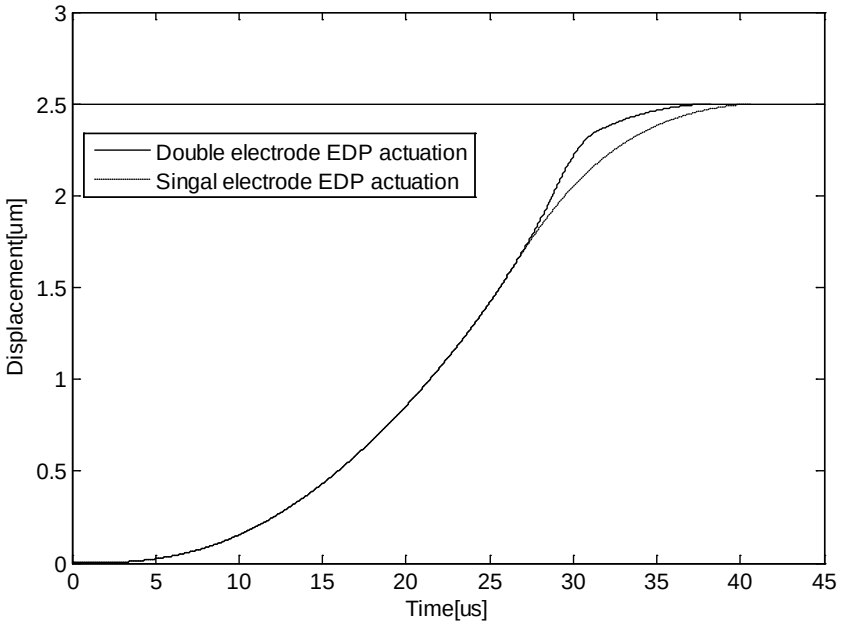

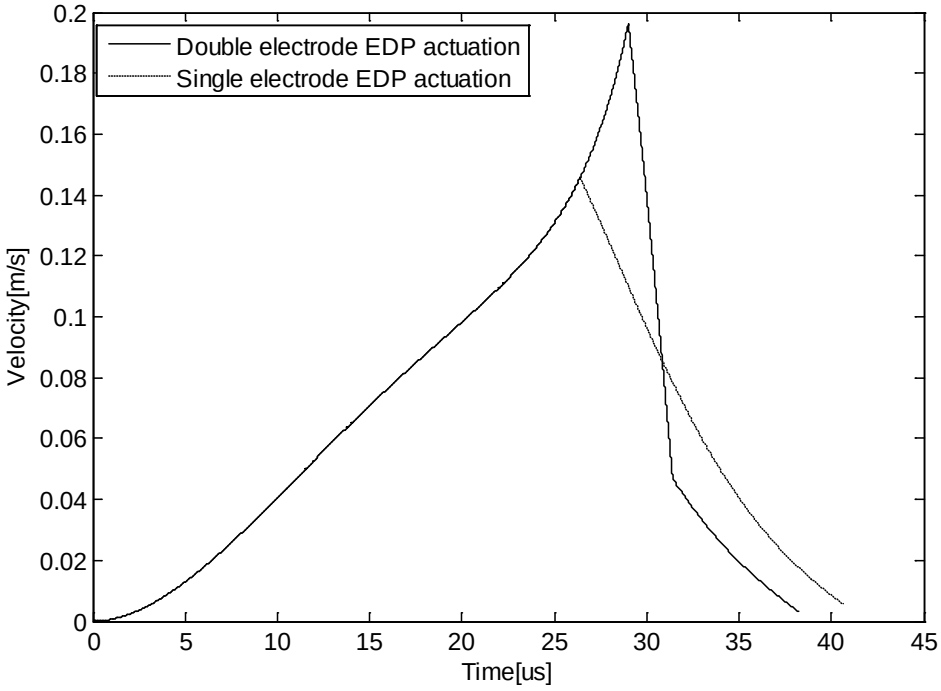

Figure 36: Landing time and landing velocity comparison for EDP and EDP using double electrodes

From figure 35, it is seen that double electrode configuration can improve beam dynamics by reducing both landing time and landing velocity for the DP waveform. The landing time reduces from *27.08 μs* to *26.8 μs* .The velocity reduction is more profound and reduces from *.055 m/s* for single electrode DP to *.022 m/s* for the double electrode configuration.

For the EDP case shown in figure 36, landing time reduction is more profound as compared to landing velocity. The landing time reduces from *41 μs* to *37 μs* .The velocity reduces from *.0053 m/s* for single electrode to *.0032 m/s* for the double electrode configuration.

Hence, for both cases we see that the double electrode model provides better overall dynamics compared to the single electrode case.

4.2 Beam Model

The parameters used in the model were taken from [2]. Table 10 shows the parameters were used for the beam model.

Table 10: Parameters for beam model

Parameter	Value
Length	70 um
Width	30um
Thickness	2um
Gap (d_g)	1.5um
Max distance d_t)	.75um
Electrode position	21 um to 49 um
Young's Modulus (E)	207GPa
Density	8900 kg/m^3

4.2.1 Bouncing Characteristics Shown Using Uncontrolled

The bouncing characteristic for the double electrode model is simulated using a Simulink model.

a) Uncontrolled Bouncing Displacement

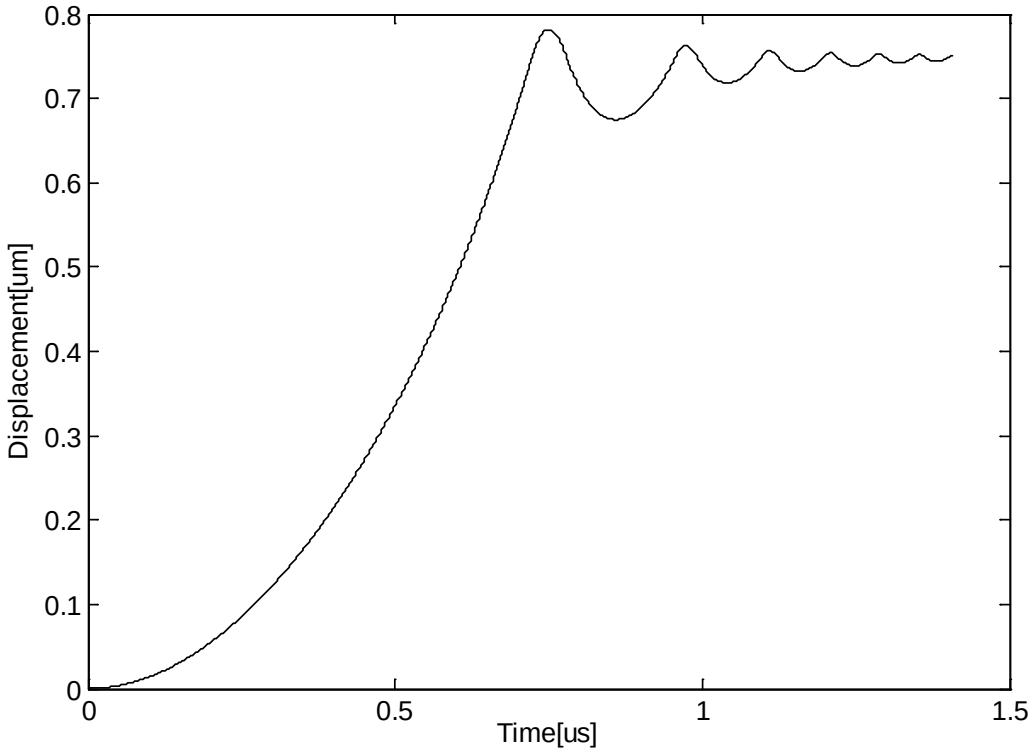

Figure 37: Uncontrolled bounce dynamics

As seen in figure (37), the bouncing occurs *at 0.75 μm* as the substrate is reached at that location. Unlike the static assumptions of damping taken in the lumped parameter model, squeeze film damping was implemented in the beam model to get more accurate representation of beam dynamics.

4.2.2 Control of Bouncing Using the Double Electrode

Similar to the beam mass model several important parameters where tested for the beam model. The parameters tested for the beam model are voltage in the

form of actuation voltage. The pulse width and pulse timing. The detailed definition for individual parameters and there significance may be found in section 4.1.2.

a) Actuation Voltage

Figure (38-39) shows the Landing velocity and time for changes in actuation voltage. The control voltage was set at *110V* .The pulse width was set at *0.21 μs* and pulse timing was *0.61 μs*.

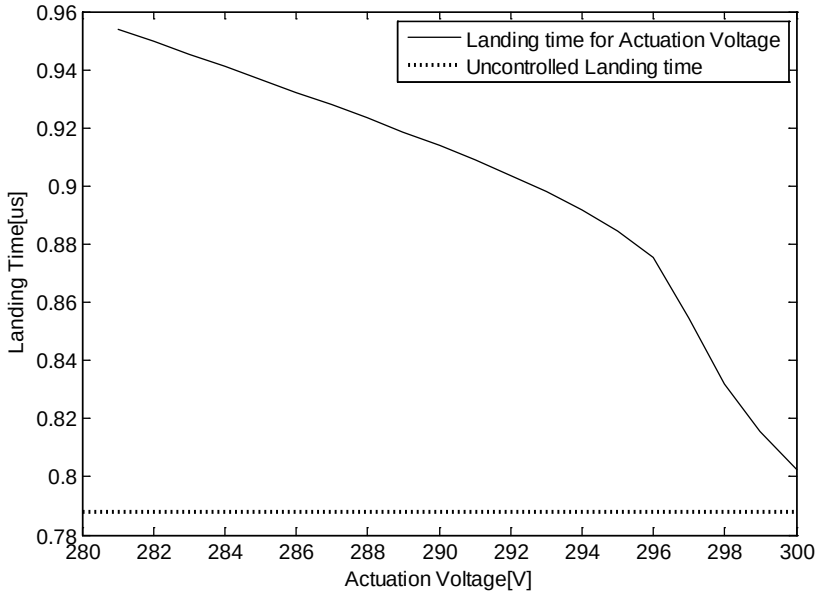

Figure 38: Landing time vs actuation voltage

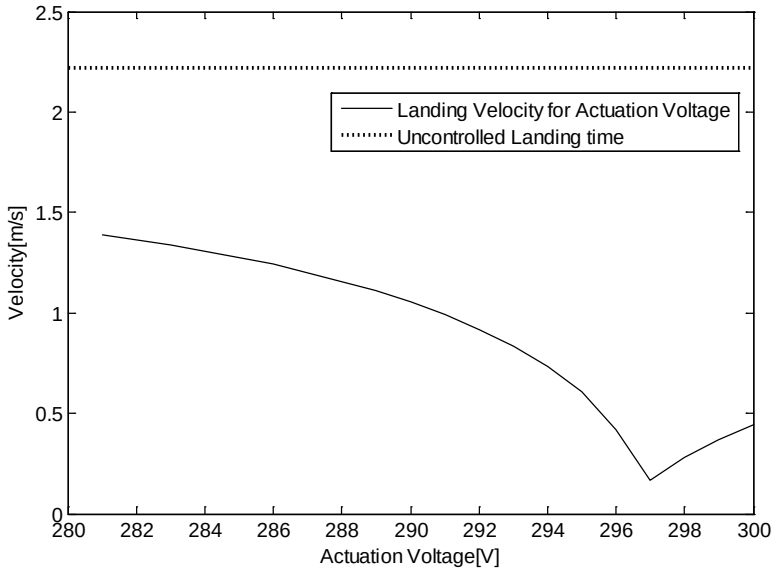

Figure 39: Landing velocity vs actuation voltage

It can be seen that the result matches the overall trend followed in lumped parameter model. Also, the lowest voltage point may be explained as in lumped parameter model using figure (25). Like actuation voltage, control voltage also follows a similar trend over a wider range of values.

b) Control Pulse Width

For this case the pulse was applied before the landing of the beam tip. The voltages are fixed at *280V* and *110V* for actuation and control respectively. The pulse timing is set at *0.61* μs. The figures (40-41) below show the landing times and velocity for different pulse widths used to test the landing time and landing velocities.

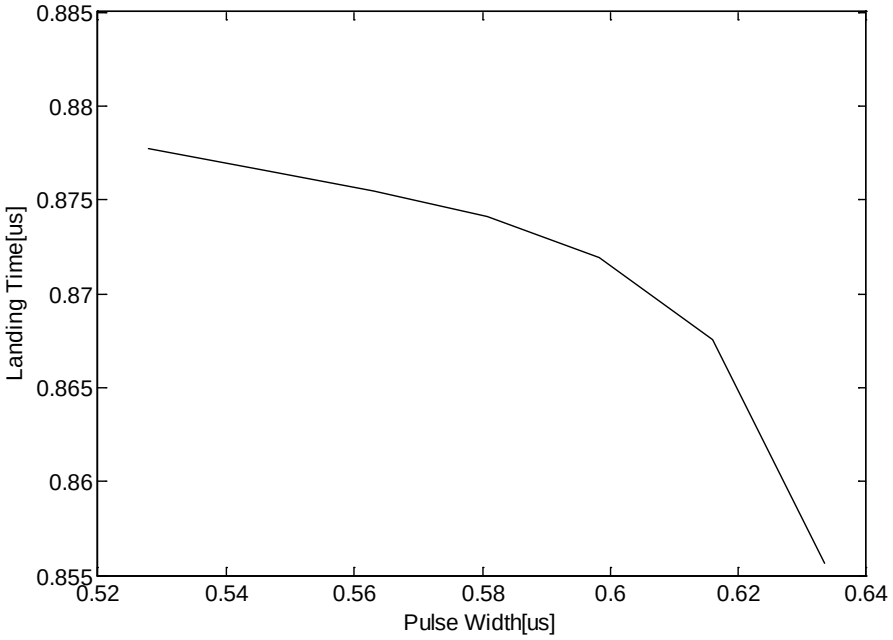

Figure 40: Landing time vs pulse width

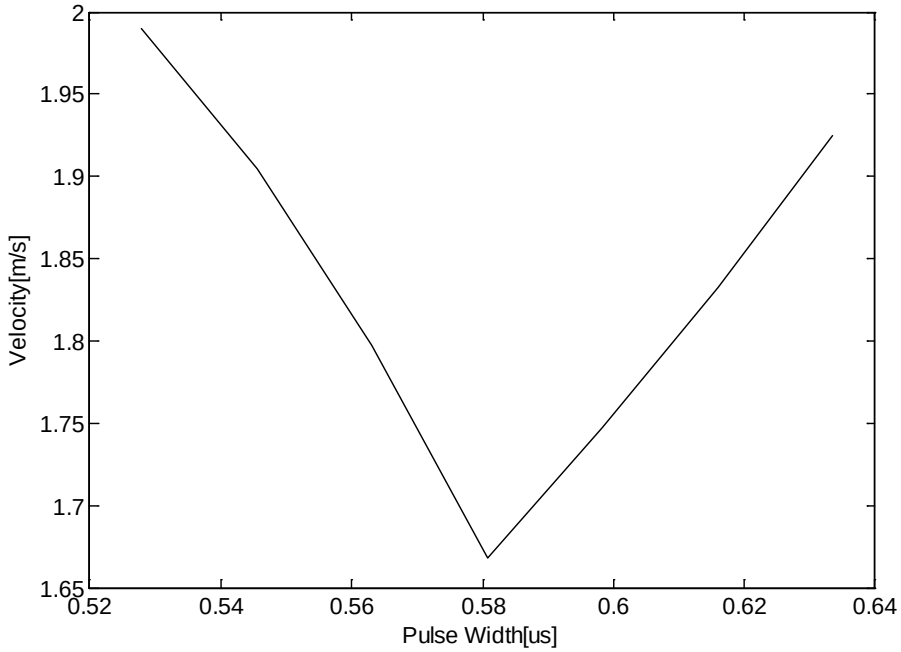

Figure 41: Landing velocity vs pulse width

As in the case of lumped parameter modeling, certain pulse width provide best landing velocity characteristics. Also, it can be seen from figure (40) and (41) smaller pulse width allow for faster landing times with sacrifice in terms of higher landing velocities. The figures verify the case for the lumped mass system.

c) Control Pulse Timing

For this simulation, Voltages is set at *280V* and *110V* for control and actuation voltages respectively. The pulse width is set to *0.21μs*. The figures below show the characteristics of the landing time and velocity for moving the pulse *.0175 μs* forward each iteration near the theoretical contact time between the tip and the substrate.

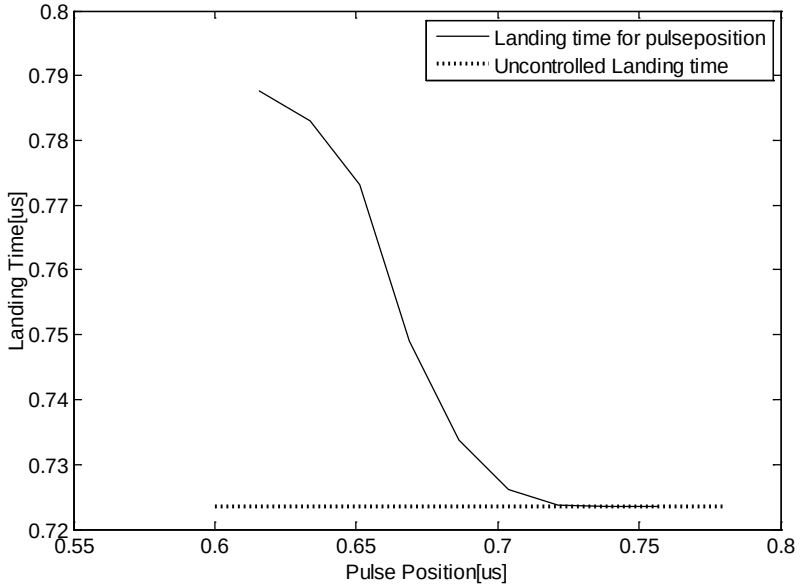

Figure 42: Landing time vs pulse position

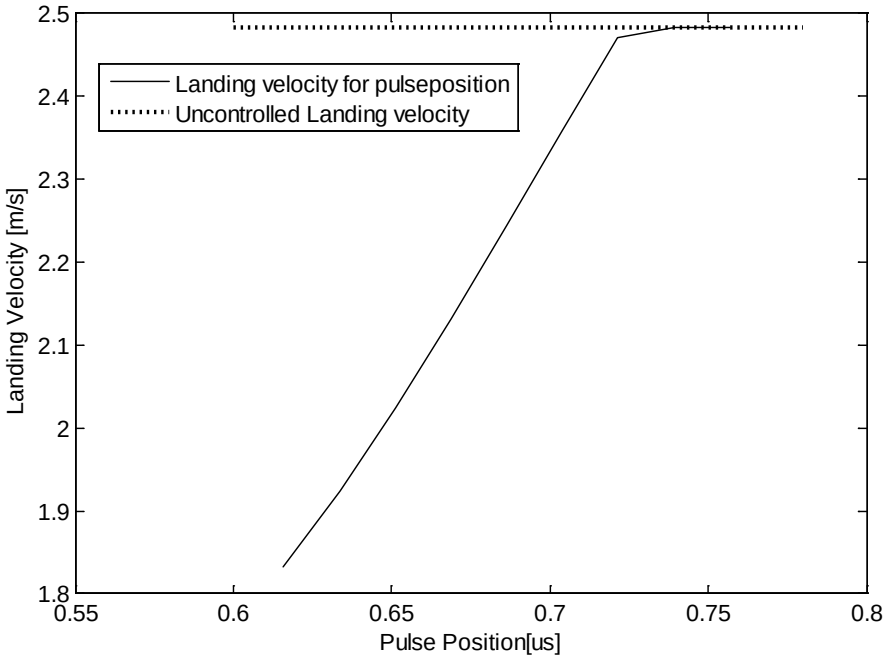

Figure 43: Landing velocity vs pulse position

As seen from figure (42-43), for a constant pulse width, velocity and landing times increase as the pulse is delayed. Both the changes in landing times and velocity are small. After the pulse passes the point where the impact first impact between the tip and the substrate occurs, then the application of the pulse no longer affects landing time and landing velocity. The results match the ones provided by the lumped mass system.

4.2.3 Tuning

Similar to the case of lumped parameter system, the system can be tuned using the above parameter to provide no bouncing. Driving an energy model for beam model is much harder. A simpler solution is to convert the beam model to a

spring mass model using the parameters provided. Then the method mention in section 4.1.3 can be applied. Figure (44) is an example of this tuning.

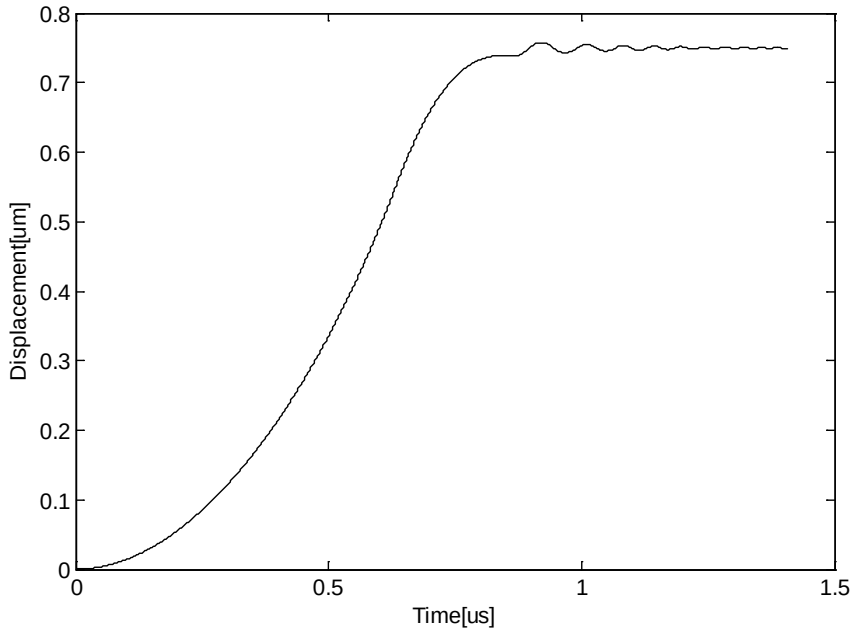

Figure 44: Tuned bouncing profile for beam model

We can see that the double electrode model matches the overall pattern for parameter change in the beam model. The differences in values are due to both systems being modeled using different sources for parameters.

Chapter 5.
Conclusion and Future Work

This thesis discusses a new technique to reduce the problem of bouncing in micro beams using the double electrode model which uses resistive forces to slow down the acceleration of the beam to ensure smooth landing time. The main idea behind the control voltage is to allow users to tune the system according to their requirements. The system was modeled using the lumped parameter model and the beam model and the dependence of several variables was tested on the system dynamics and schemes were developed to allow for better control. The results were compared against popular bouncing control waveforms to show the viability of the double electrode control scheme. Finally, the beam model was used to verify the lumped mass model to ensure parameters tested followed similar trajectory in both cases. The overall simulations result show positively that bouncing and landing time maybe reduced overall by the application of a resistive force using a double electrode configuration.

The next step on continuing of this research is to fabricate the beam and experimentally show that no bounce can be obtained by varying the control parameters. Energy methods can be used to further study the system and provide methods to derive best parameters where other analytical solutions have failed. Analytical methods such as the differential flatness methods can also be implemented to reduce the complexity of the nonlinear system and provide optimization of important parameters while ignoring less important ones.

BIBLIOGRAPHY

[1] H. Sumali, J. E. Massad, D. A. Czaplewski, and C. W. Dyck, "Waveform design for pulse-and-hold electrostatic actuation in MEMS," Sensors and Actuators A: Physical, vol. 134, pp. 213-220, 2/28/ 2007.

[2] B. McCarthy, G. G. Adams, N. E. McGruer, and D. Potter, "A dynamic model, including contact bounce, of an electrostatically actuated microswitch," Microelectromechanical Systems, Journal of, vol. 11, pp. 276-283, 2002.

[3] C. Do, M. Lishchynska, M. Cychowski, K. Delaney, and M. Hill, "Energy-based approach to adaptive pulse shaping for control of RF-MEMS DC-contact switches," 2012.

[4] D. A. Czaplewski, C. W. Dyck, H. Sumali, J. E. Massad, J. D. Kuppers, I. Reines, et al., "A soft-landing waveform for actuation of a single-pole single-throw ohmic RF MEMS switch," Microelectromechanical Systems, Journal of, vol. 15, pp. 1586-1594, 2006.

[5] J. C. Blecke, D. S. Epp, H. Sumali, and G. G. Parker, "A Simple Learning Control to Eliminate RF-MEMS Switch Bounce," Journal of Microelectromechanical Systems, vol. 18, pp. 458-465, Apr 2009.

[6] C. Lai and W. S. Wong, "A comparison between voltage waveforms to enhance the lifetime of MEMS switch," in IECON 2011-37th Annual Conference on IEEE Industrial Electronics Society, 2011, pp. 2082-2087.

[7] A. Peschot, C. Poulain, N. Bonifaci, and O. Lesaint, "Contact bounce phenomena in a MEM switch," in Electrical Contacts (Holm), 2012 IEEE 58th Holm Conference on, 2012, pp. 1-7.

[8] R. C. Tung, A. Fruehling, D. Peroulis, and A. Raman, "Multiple Timescales and Modeling of Dynamic Bounce Phenomena in RF MEMS Switches," 2014.

[9] A. Jain, P. R. Nair, and M. A. Alam, "Strategies for dynamic soft-landing in capacitive microelectromechanical switches," Applied Physics Letters, vol. 98, pp. 234104-234104-3, 2011.

[10] M. Spasos and R. Nilavalan, "On the investigation of a reliable actuation control method for ohmic RF MEMS switches," Microelectronics Journal, vol. 42, pp. 1239-1251, 2011.

[11] H. F. Dadgour, M. M. Hussain, C. Smith, and K. Banerjee, "Design and analysis of compact ultra Energy-Efficient logic gates using laterally-actuated double-electrode NEMS," in Design Automation Conference (DAC), 2010 47th ACM/IEEE, 2010, pp. 893-896.

[12] M. I. Younis, MEMS Linear and Nonlinear Statics and Dynamics: Mems Linear and Nonlinear Statics and Dynamics vol. 20: Springer, 2011.

[13] W. S. Wong and C. Lai, "Mitigation of MEMS Switch Contact Bouncing: Effectiveness of Dual Pulse Actuation Waveforms and Robustness Against Variations in Switch and Waveform Parameters," Sensors and Actuators A: Physical, 2013.

[14] S. Pamidighantam, R. Puers, K. Baert, and H. A. Tilmans, "Pull-in voltage analysis of electrostatically actuated beam structures with fixed–fixed and fixed–free end conditions," Journal of Micromechanics and Microengineering, vol. 12, p. 458, 2002.

[15] S.-W. Lee, R. Johnstone, and A. M. Parameswaran, "MEMS mechanical logic units: design and fabrication with micragem and polymumps," in Electrical and Computer Engineering, 2005. Canadian Conference on, 2005, pp. 1513-1516.

[16] W. W. Jang, O. D. Kwon, J. O. Lee, and J.-B. Yoon, "Microelectromechanical (MEM) switch and inverter for digital IC applications," in Solid-State Circuits Conference, 2007. ASSCC'07. IEEE Asian, 2007, pp. 256-259.

[17] C.-Y. Tsai, W.-T. Kuo, C.-B. Lin, and T.-L. Chen, "Design and fabrication of MEMS logic gates," Journal of Micromechanics and Microengineering, vol. 18, p. 045001, 2008.

[18] S. Chakraborty, A. R. Chaudhuri, and T. K. Bhattacharyya, "Design and analysis of MEMS cantilever based binary logic inverter," in Proceedings of the 2009 International Conference on Advances in Computing, Control, and Telecommunication Technologies, 2009, pp. 184-188.

[19] F. M. Alsaleem and M. I. Younis, "Stabilization of electrostatic MEMS resonators using a delayed feedback controller," Smart Materials and Structures, vol. 19, p. 035016, 2010.

[20] S. Chakraborty and T. K. Bhattacharyya, "Development of MEMS based universal gate for signal processing circuit in low frequency sensor applications," in Students' Technology Symposium (TechSym), 2010 IEEE, 2010, pp. 129-136.

[21] H. F. Dadgour, M. M. Hussain, C. Smith, and K. Banerjee, "Design and analysis of compact ultra energy-efficient logic gates using laterally-actuated double-electrode NEMS," in Design Automation Conference (DAC), 2010 47th ACM/IEEE, 2010, pp. 893-896.

[22] T.-J. K. Liu, J. Jeon, and H. Kam, "Prospects for MEM logic switch technology," 2010 International Electron Devices Meeting, pp. 18.3. 1-18.3. 4, 2010.

[23] C.-Y. Tsai and T.-L. Chen, "Design, fabrication and calibration of a novel MEMS logic gate," Journal of Micromechanics and Microengineering, vol. 20, p. 095021, 2010.